Synthesis and Characterization of Polyhedral Oligomeric Silsesquioxane (POSS) Based Amphiphiles

Yang Liu

Thesis submitted to the Faculty of the Virginia Polytechnic Institute and State University in partial fulfillment of the requirements for the degree of

Master of Science

in

CHEMISTRY

Alan R. Esker, Chair

Richard D. Gandour

John R. Morris

Dec 6, 2010

Blacksburg, VA

Keywords: POSS, air/water (A/W) interface, Π–*A* isotherms, Brewster angle microscopy (BAM), Langmuir films

Synthesis and Characterization of Polyhedral Oligomeric Silsesquioxanes (POSS) Based Amphiphiles

Yang Liu

ABSTRACT

Polyhedral oligomeric silsesquioxanes (POSS) have attracted substantial academic interest for many years as hybrid materials and nanofillers for controlling thermal and mechanical properties, and for providing thermal and chemical resistance while retaining ease of processing. A natural extension of these studies has been working on POSS-based amphiphiles and thin film coatings. Studies at the air/water (A/W) interface have shown that trisilanol-POSS derivatives are amphiphilic and form uniform Langmuir films, whereas closed-cage POSS derivatives are hydrophobic and aggregate.

In this study, two novel POSS derivatives were synthesized from PSS-(3-hydroxypropyl)-heptaisobutyl substituted (POSS-OH) and completely characterized. Weisocyanate reacted with POSS-OH, and a POSS-based triester (POSS-triester) was obtained. Trifluoroacidolysis of the POSS-triester at room temperature afforded the corresponding triacid (POSS-triacid). Purified POSS-OH, POSS-triester, and POSS-triacid were studied by using surface pressure – area per molecule (Π-*A*) isotherms as well as Brewster angle microscopy (BAM) at the air/water (A/W) interface. Compared with previous work on trisilanol-POSS derivatives, the results indicated that POSS-triester was surface active and formed a liquid-expanded (LE) monolayer. In contrast, POSS-triacid monolayers were more condensed (LC) and were not dramatically affected by changes in pH. Results for the lift-off areas ($A_{lift\text{-}off}$), limiting areas (A_0), collapse areas (A_c), and

collapse pressures (Π_c) of POSS-OH, POSS-triester, and POSS-triacid were compared to trisilanolisobutyl-POSS (TiBP) and were interpreted in terms of possible molecular conformations. Whereas, TiBP has been hypothesized to exist in a vertex-on conformation, POSS-OH and POSS-triacid packing at the A/W interface was consistent with face-on conformations. For POSS-triester, the isotherm was consistent with a vertex-on conformation at low Π, but a face-on conformation at high Π.

To my entire family who have been supportive at all times.

ACKNOWLEDGEMENTS

I would like to extend heartfelt thanks to my advisor, Dr. Alan R. Esker for accepting me into his group and giving me opportunities to work in my interest area with precious counsel. I would like to thank Dr. Richard D. Gandour and Dr. John R. Morris for serving on my research committee. Additionally, I would like to thank Dr. Gandour for all of his help with the synthetic aspects of my project. I would also like to thank Dr. Herve Marand Dr. Louis P. Madsen, for their generous guidance.

I would like to thank my colleagues in Dr. Esker's group who make my research joyful and successful: Dr. Soulong Ni, Dr. Bingbing Li, Dr. Rituparna Paul, Dr. Ufuk Karabiyik, Dr. Wojin Lee, Dr. Wen Yin, Dr. Adulaziz Kaya, Dr. Qiongdan Xie, Jae-Hyun Sim, Zelin Liu, Chuanzi Ou-Yang, Xiaosong Du, Joshua Kittle, Xijing Yuan, Chao Wang, Xiao Zhang, David, Caldwell, Heejun Choi, and Liz Huh. I would like to thank Dr. Guangbin Wang, Dr. Min Mao, Dr. Yanpeng Hou, Dr. Ting Cai, Dr. Nan Dai, Dr. Liangming Hu, Ronald Chen, Grace Xu, Bin Zhang, Anderson Sun, and Yi Li for their help without reservation when I have questions. I would also extend special thanks to Jianfei Zhang, Liaosa Xu, Dr. Wujun Fu, Jielu Zhao, Ende Pan, and Jianyuan Zhang, for their friendship which makes my spare time in Blacksburg colorful.

I would like to thank my parents and brother for their love and support. I would like to dedicate this thesis to my grandma who passed a month ago. At last, I would like to thank my wife, Changqin Chen, who sacrificed her career for me. Thanks for her trust and sharing, especially in my hard times. I cannot imagine my journey through life without her.

TABLE OF CONTENTS

LIST OF FIGURES

Chapter 1

Chapter 2

Chapter 3

Chapter 4

LIST OF SCHEMES

Chapter 1

Chapter 2

Chapter 4

Chapter 1

Introduction and Literature Review

1.1 Introduction to Interfaces and Colloids

Interfaces, the areas which separate two phases from each other, generally include the solid-liquid, the solid/gas, and the liquid-gas interfaces. Since the boundary between water and oil can be distinguished as two immiscible liquids, liquid/liquid interfaces are also studied as well as solid/solid interfaces. However, gas/gas interfaces are not considered because all gases are miscible. Collides, usually discussed with interfaces, are disperse systems, with dispersed phase lateral dimensions on the order of nm to μm.[1] Colloids and interfaces are intimately related since the interface-to-volume ratio is so large that their behavior is critically dependent upon the surface properties. For this reason, some properties of nanoscience and nanotechnology are intimately related to interfacial behavior as properties deviate from their bulk values.

Interest in interfaces and colloids has developed in a variety of areas including lipid membranes in biology,[2] swelling of clay or soil in geology,[3] butter manufacturing in food science,[4] detergency,[5] thin films,[6] coatings,[7] paints,[8] etc. However, a surface is seldom an infinitesimally sharp boundary in the direction of its normal; rather it is rough, and this roughness affects properties and applications. In this thesis, the air/water (A/W) interface is the main interface. The density of a liquid surface decreases from its bulk value to its vapor value over a few molecular diameters.[9]

1.2 Introduction to Polyhedral Oligomeric Silsesquioxanes (POSS)

Polyhedral oligomeric silsesquioxanes are more commonly known as POSS. These compounds have attracted substantial academic interest for many years as a hybrid material.[10] POSS is composed of a relatively hard 0.5 nm diameter inorganic core and that makes the overall diameter of the molecules 1 to 3 nm. The two most common types of POSS are closed-cage POSS and open-cage POSS (Figure 1.1). Of the closed-cage POSS derivatives, the one composed of eight silsesquioxane units (T_8) is the most common. While octaalkyl-POSS derivatives are normally hydrophobic, open cage trisilanol-POSS derivatives are amphiphilic. Since the octaalkyl-POSS can be synthesized from a trisilanol-POSS, opportunities to build molecules with different rigidities and amphiphilic properties in nanoscale dimensions exist.[10a] POSS has attracted considerable interest for high-temperature nanocomposites, space-survivable coatings,[10b] low-*k* dielectric materials,[10c] liquid crystalline polymers,[10d] and catalysts.[10e] Varieties of POSS-based polymers have been made and have shown interesting properties.[10f-i] Such hybrid materials have properties between inorganic and organic compounds with respect to glass transition temperature, mechanical strength, thermal and chemical resistance, and ease of processing.[10j]

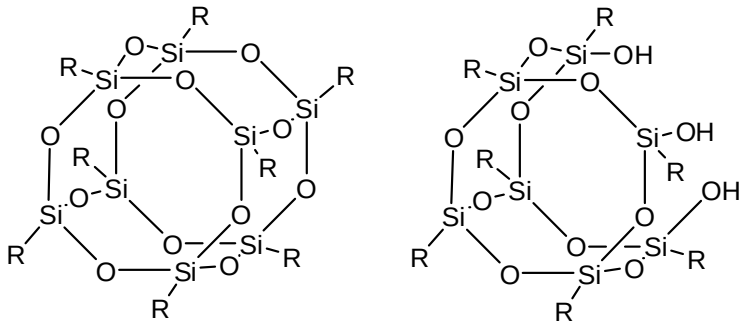

Octaalkyl-POSS Trisilanol-POSS

Figure 1.1 Two most common types of POSS. R = alkyl group.

1.2.1 POSS Cage Synthesis

A silsesquioxane has a general empirical chemical formula $RSiO_{1.5}$, in which R is hydrogen or an alkyl, alkene, aryl, or arylene group. However, substituents are not necessarily the same on every Si atom. Frequently, one substituent on closed-cage POSS derivatives has a more branched arm that ends with a functional group, such as an alcohol, amine, alkene, etc.

Synthesis of the POSS cages requires hydrolytic condensation. POSS derivatives have been formed from trialkoxysilanes and trichlorosilanes ($RSiX_3$) (Scheme 1.1 and 1.2).[11] In order to obtain different POSS derivatives, the reaction rate is controlled with a catalyst or by the choice of solvent.

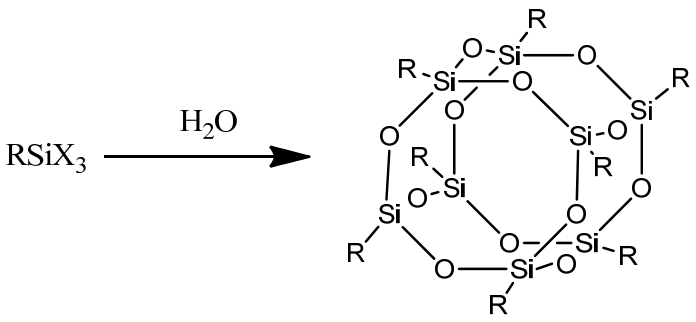

Scheme 1.1 Scheme for synthesizing closed-cage POSS derivatives.[11]

Problems with Scheme 1.1, where R is usually a chemically stable organic substituent or H, include the need to carefully control the initial concentration of the monomer and catalyst, the temperature, the rate of addition of water, etc.[11-12] The character of the substituent X and solubility of polyhedral oligomers can also influence the rate and distribution of products for the reaction in Scheme 1.1.[10a] For example, higher temperature tends to favor polymer formation;

hence room temperature reactions under mild conditions are normally preferred. Furthermore, dropwise addition of H_2O is suggested to control the concentration of silanol groups to avoid extensive side reactions (such as branched oligomers and linear polymers). Different solvents (such as cyclohexane, benzene, methanol, and acetone) and catalyst (either HCl or KOH) have been used depending on the organic substituents.[13]

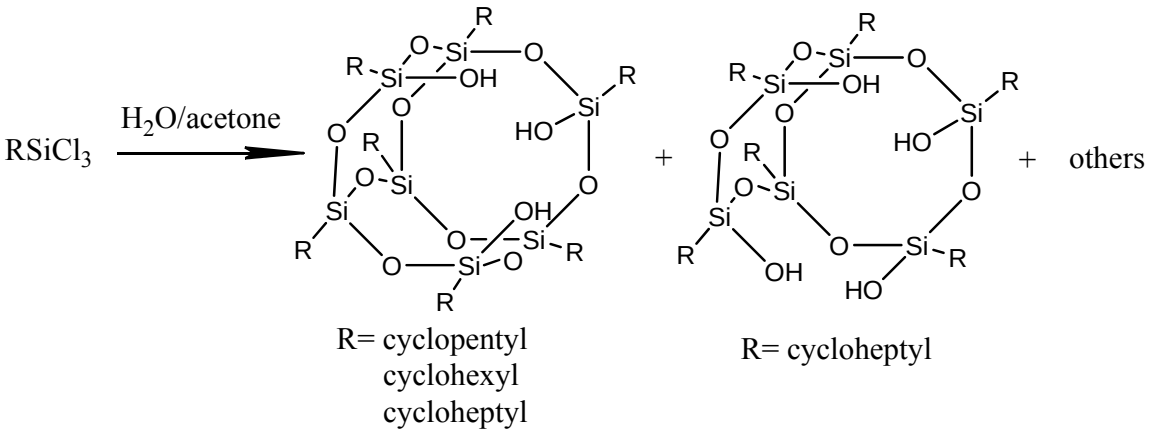

Scheme 1.2 Scheme for synthesizing open-cage POSS derivatives.[11]

Open cage trisilanol POSS derivatives are one example of a series of incompletely condensed POSS cages. Here, an open cage POSS means that at least one hydroxyl group exists with at least one missing vertex. Feher and his coworkers[14] have designed a method to control the reactivity of the monomer $RSiX_3$ to synthesize opened cage POSS (Scheme 1.2). By introducing acetone, it was possible to slow the hydrolytic condensation when R was a cyclopentyl or cyclohexyl group. However, these reactions usually took a few days and the yields were relatively low (< 30%). Later, strong acids proved to be effective for the selective cleavage of completely condensed octameric polyhedral silsesquioxane ($R_8Si_8O_{12}$) cubes (Scheme 1.3).[15]

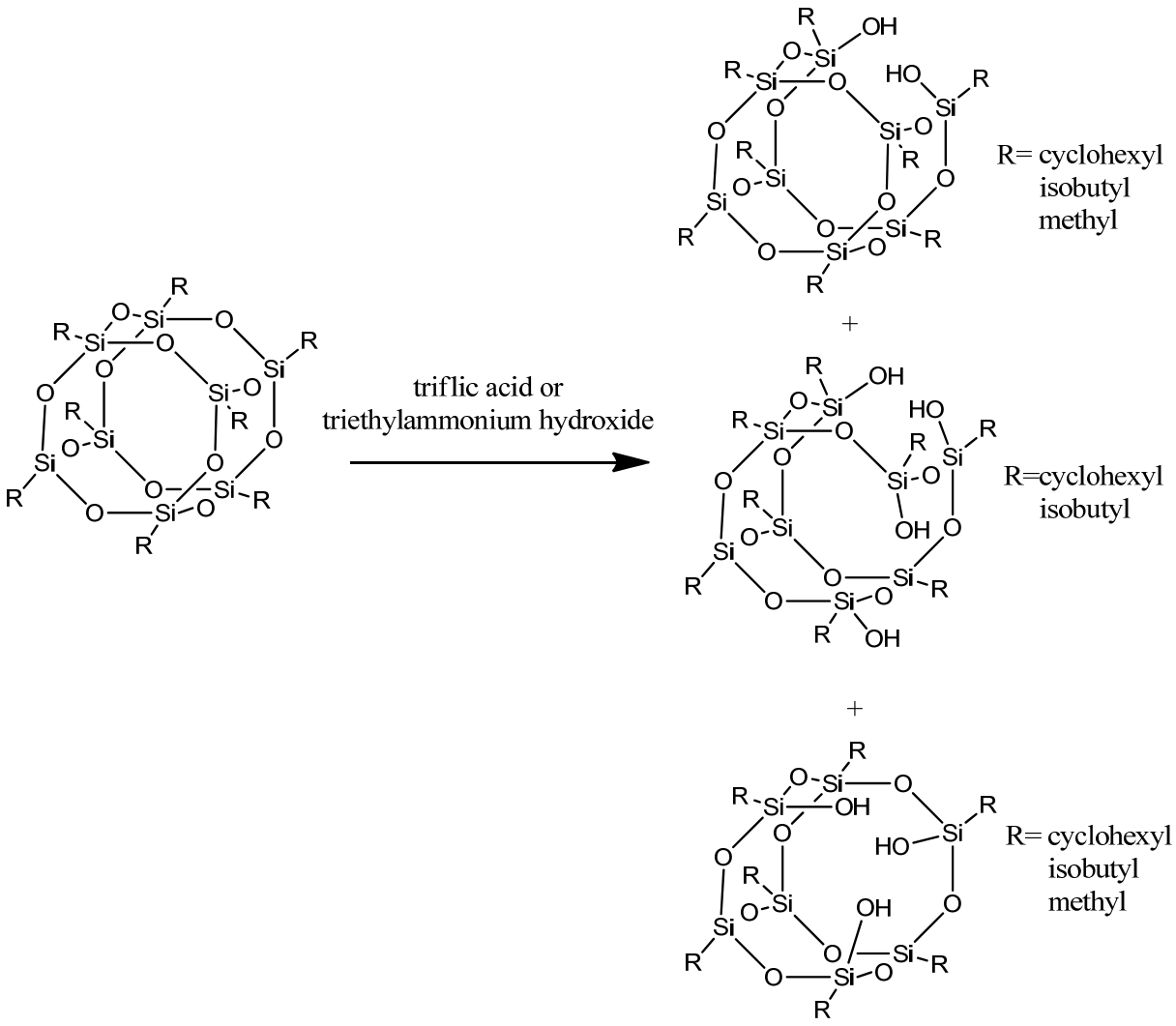

Scheme 1.3 Synthesis of incompletely condensed POSS cages from the cleavage of completely condensed POSS in the presence of an acid or base catalyst.

1.2.2 Synthesis of POSS-based Polymers

As an organic/inorganic hybrid material, POSS is of interest for blends with polymers or dendrimers. These blends tend to exhibit increases in use temperature, reductions in flammability, better oxidation resistance, and surface hardening.[16] One major advantage for POSS in these potential applications is the ability to tailor the POSS cage in order to control blending with polymers.[17] The physical properties of these hybrid materials depend on the miscibility of the host polymer and the POSS derivative.[18]

Polyaddition and polycondensation are common methods for the synthesis of POSS-based polymers.[19] One interesting study used epoxy-functionalized cubes, octaaminophenylsilsesquioxane (OAPS), polyaminophenylsilsesquioxane (PAPS), octa(dimethylsiloxypropylglycidyl ether) silsesquioxane (OG), diaminodiphenylmethane (DDM), and diglycidyl ether of Bisphenol A (DGEBA) to create nanocomposites.[20] For the resulting nanocomposite, it was believed that the rigidity, processability and thermomechanical properties could be improved by adjusting the architecture of the organic tethers between vertices.[21] Many examples of asymmetric POSS derivatives derived from an octafunctional-POSS have been studied.[10d, 22]

1.2.3 Physical Properties and Applications of POSS

As a hybrid material, POSS is a bridge between ceramics and polymers. Compared to conventional organic and inorganic materials, it has intermediate properties with respect to use temperature, oxidation resistance, toughness, density and ease of processing. POSS has tremendous potential as a space survival material based on its low density, reduced heat

evolution and good oxidation resistance, and as case insulation for solid rocket engines and ducting for liquid rocket engines.[23] In order to achieve these properties, control of molecular weight and composition led to the modification of open-caged POSS derivatives to create polymerizable and crosslinkable units for the development of model silica surfaces,[24] building blocks for network solids,[25] and ligands.[12a, 26]

The morphology of POSS-based polymers has attracted greater attention. Crystalline polymers, such as polynorbornene[27] and poly(lactide-co-glycolide) (PLGA)[28] were introduced into POSS segments. Compared to the earlier work done on block copolymers with amorphous POSS segments,[29] the nanoconfinement effect within microphase-separated domains highly depended upon the state of the POSS. The POSS-rich domains mainly acted as crosslinks, however, "pseudo-network" systems were sometimes observed during physical aging experiments.[30] Many techniques have been used to examine the morphology of POSS-containing copolymers. For example, wide-angle X-ray scattering (WAXS) was used to investigate POSS-based ABA triblock microstructures[31] and the intermediate ordering of POSS homopolymer.[32] Transmission electron microscopy (TEM) and dynamic mechanical analysis (DMA) were also used to study phase-separated microstructures with different POSS components.[31]

Open cage POSS derivatives are surface active and closed-cage POSS derivatives can also be coupled with hydrophilic polymers to create amphiphilic materials. These new materials usually exhibit an affinity for interfaces, which makes them potential compatibilizers and dispersion aides. POSS is also excellent model nanofiller with well-defined size. The Esker group has demonstrated an increase in the T_g of polymeric thin films with small amounts of trisilanolphenyl-POSS (TPP).[33] Meanwhile, different filling behaviors based on different POSS

derivatives were also examined at the A/W interface. For example, when trisilanolisobutyl-POSS (TiBP) is benlded with polydimethylsiloxane (PDMS), TiBP was believed to platicize the blend films at low surface pressure, thereby reducing mechanical strength.[34] TPP could also form thin film bilayers and thin film blends with polymers leading to interesting morphological behavior.[35] For example, thin film bilayers of polystyrene (PS) and TPP were studied with respect to morphological evolution during annealing at elevated temperatures. The dewetting mechanism in work by Paul *et al.* was different from similar studies with polymer/polymer bilayers.[36] These results indicate that dewetting of both the upper TPP and the lower PS layers led to the exposure of the silicon substrate.[35b]

Topological constraints in POSS-based polymers also affect physical properties. For example, molecular motion associated with network junctions slowed when the weight percentage of epoxy-POSS increased in the blend with diglycidyl ether of bisphenol A (DGEBA) and 1,4-butanediol diglycidyl ether (BDGE).[37] Fu *et al*. increased the rubbery plateau modulus by introducing trisilanolphenyl-POSS into the tetraglycidyl diamino diphenyl methane / 2-methyl-1,5-pentadiamine (TGDDM) / (MPDA) system.[38]

1.3 Experimental Techniques

The objective of my research is the synthesis of a triester (POSS-triester) and a triacid (POSS-triacid) from PSS-(3-hydroxypropyl)-heptaisobuyl (POSS-OH). The Langmuir-Blodgett (LB) and associated techniques will be used to study the phase behavior of POSS derivatives at the A/W interface. In order to study the morphology of amphiphilic molecules, Brewster angle microscopy (BAM) is coupled with a Langmuir trough.

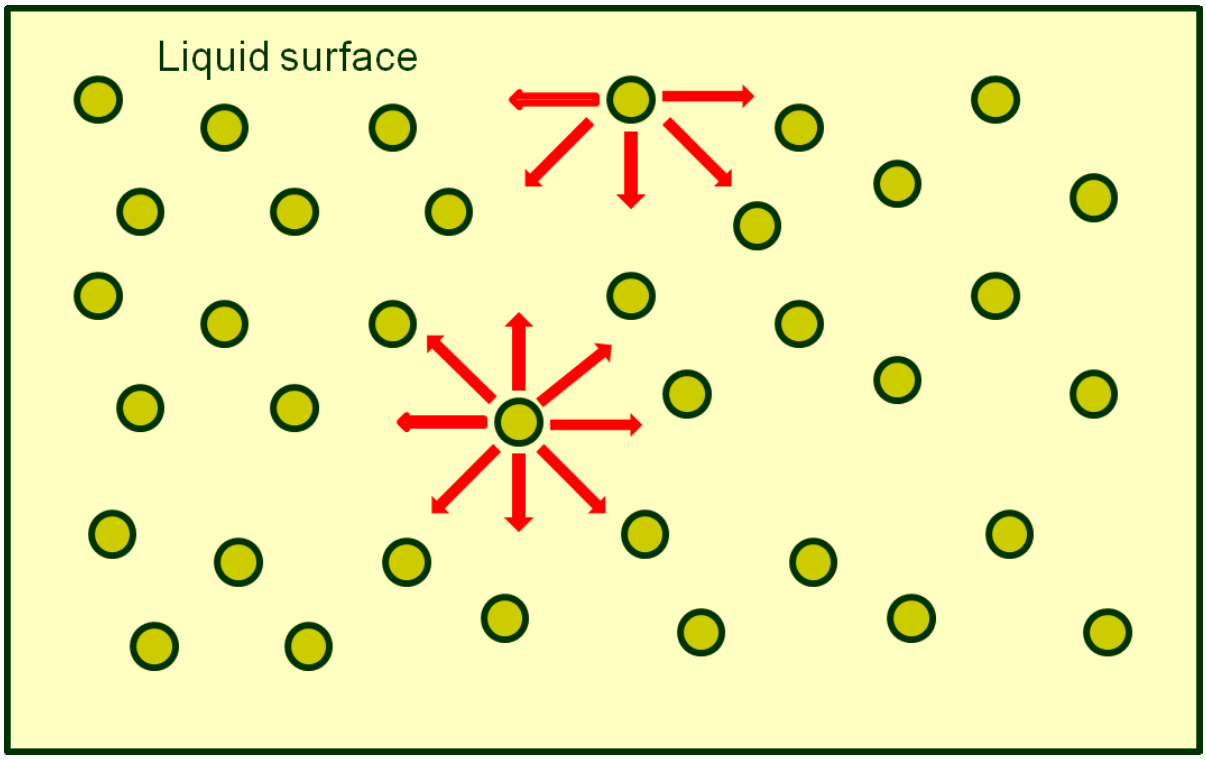

Figure 1.2 Diagram of the forces on two liquid molecules, one in the bulk versus one at the surface. Orange arrows highlight attractive forces acting on a given molecule. [39]

1.3.1 Surface Pressure-Area per Molecule (Π-*A*) Isotherms and the Langmuir-Blodgett (LB) Technique

Surface tension is a critical property of a liquid caused by cohesive forces between molecules. This effect is depicted in Fiugre 1.2. For molecules within the bulk liquid, forces experienced on the molecules are symmetrical resulting in a net force of zero. These forces include van der Waals forces, hydrogen bonding, dipolar interactions, etc. Without these attractions there would not be a condensed phase. However, for molecules located at the interface, forces are not

balanced and result in a net attractive force that pulls molecules at the surface of a liquid towards the bulk. In order to bring a molecule from the bulk to the surface, a "surface free energy" penalty represented by the surface tension or surface energy (γ) is required. This surface tension with a unit of force per unit length can also be considered as surface energy density (energy per unit area), reflecting the tendency of liquids to reduce their surface area. At thermodynamic equilibrium, the surface tension of a planar interface can be expressed as:[40]

$$\gamma = \left(\frac{\partial F}{\partial A}\right)_{T,V,n} \; or \; \gamma = \left(\frac{\partial G}{\partial A}\right)_{T,p,n} \tag{1.1}$$

where T, P, and V are temperature, pressure, and volume, respectively, *A* is the surface area, and *F* and *G* are the Helmholtz and Gibbs free energies, respectively. In this thesis, only water is discussed because it is not only the most frequently used liquid, but it also has a higher surface tension (about 73 $mN \cdot m^{-1}$ at 20 ^{o}C) than traditional organic liquids. The larger γ arises from strong hydrogen bonding between H_2O molecules.

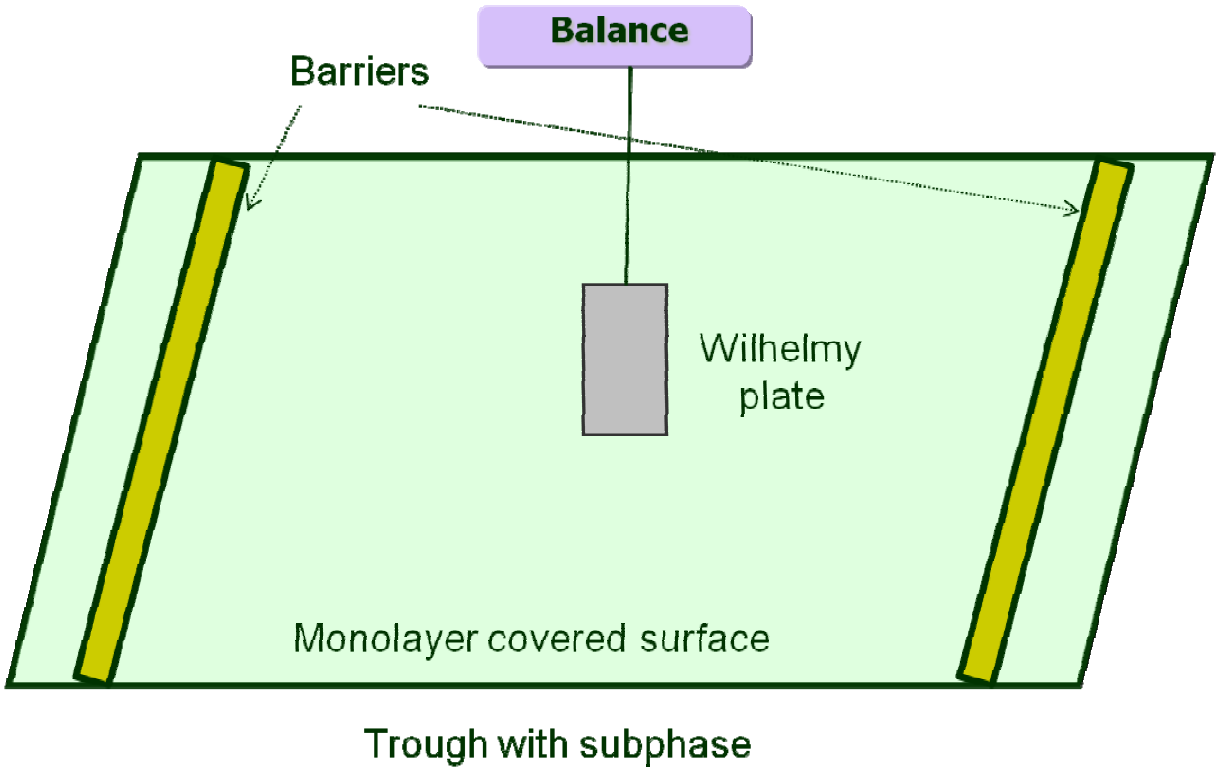

Figure 1.3 Schematic depiction of a Langmuir trough.

A Langmuir-trough (Figure 1.3) is a laboratory instrument used to study the properties of amphiphilic molecules. The instrument can be used to compress the monolayer to create a surface pressure-area per molecule (Π–*A*) isotherm. With the addition of a dipper and dipping well, a Langmuir trough becomes a Langmuir-Blodgett (LB) trough that allows the deposition of LB-films onto solid substrates. The instrument is named after Irving Langmuir and Katherine B. Blodgett, who demonstrated it was possible to create monomolecular coatings on surfaces of water, metal, and glass.[41] Films on water have become known as Langmuir films while films transferred to solid substrates by vertical deposition are known as LB-films.

Monolayers on water are usually composed of amphiphilic molecules with hydrophilic heads and hydrophobic tails.[42] Most of the early work involving Langmuir monolayers was conducted with long-chain carboxylic acids (such as stearic acid), which contain a polar headgroup anchoring the molecules to the surface of water and a hydrophobic tail preventing dissolution of the molecule. These amphiphilic molecules are also known as surfactants, since they lower the surface tension of water and allow easier spreading of the liquid on another liquid or solid. As the monolayer molecules are compressed, their steric or repulsive interactions generate a force that counteracts the contracting tendency of the liquid, thereby further lowering the surface tension. This change in the surface tension is usually called the surface pressure, $\Pi = \gamma_{liquid} - \gamma_{film}$, where γ_{liquid} is the surface tension of the neat liquid and γ_{film} is the surface tension of the liquid with a surface film. Π can be considered as the two-dimensional (2D) analog of a three-dimensional (3D) bulk pressure (P). Semi-quantitatively, Π can be thought of as a pressure distributed over the thickness of the thin film:

$$P(mN \cdot m^{-2}) = \frac{\Pi(mN \cdot m^{-1})}{thickness(m)} \tag{1.2}$$

Likewise, a 2D lateral modulus, ε_s (to be discussed later):

$$\varepsilon_s = -A\left(\frac{\partial \Pi}{\partial A}\right)_T \tag{1.3}$$

can be considered as an analog of the 3D bulk modulus, K:

$$K = -V\left(\frac{\partial P}{\partial V}\right)_T \tag{1.4}$$

In these studies, the amphiphilic molecules are normally dissolved in a spreading solvent (chloroform, dichloromethane, hexane, etc.). The solvent chosen must have a positive spreading coefficient:

$$S = \gamma_{air/water} - \gamma_{air/solvent} - \gamma_{solvent/water} \quad (1.5)$$

where $\gamma_{air/water}$, $\gamma_{air/solvent}$ and $\gamma_{solvent/water}$ correspond to the interfacial tensions between air and water, air and solvent, and the spreading solvent and water, respectively.[43] Ideally, the spreading solution is deposited onto the surface of the trough to disperse the material in a monomolecular state.

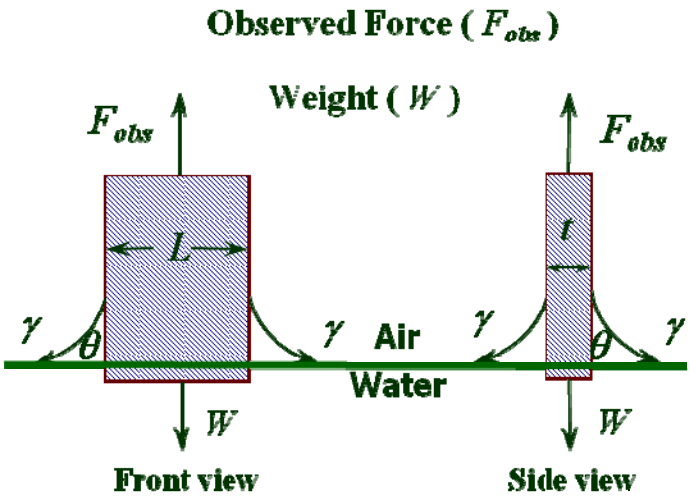

Figure 1.4 Measurement of surface pressure with a Wilhelmy plate.

The aqueous subphase is normally placed in a trough made of a hydrophobic material, like Teflon. Π can be monitored by the Wilhelmy plate method (Figure 1.4). In the Wilhelmy plate method, absolute forces acting on the plate, usually made of roughened platinum or filter paper,

and partially immersed in the subphase, are measured. Downward forces working on the plate, such as gravity and surface tension, are balanced by upward forces, such as buoyancy, resulting from the displacement of water by the plate, and the pressure sensor itself. These forces are usually measured with a sensitive electrobalance.[44] γ and Π can be calculated from:

$$\Pi = \gamma_0 - \gamma_{film} = \frac{F_{obs,0} - F_{obs,film}}{2(L+t)\cos\theta} \tag{1.6}$$

where γ_0 is the surface tension of the pure liquid and γ_{film} is the surface tension of the film covered surface. $F_{obs,0}$ is the force measured by the Wilhelmy plate when there is no Langmuir film on the surface, $F_{obs,film}$ is the force measured by the Wilhelmy plate when there is a Langmuir film on the surface, L is the length of the plate, t is the thickness of the plate, which is usually small relative to L and is frequently ignored, and θ is the contact angle between the water and the Wilhelmy plate.

The contact angle is the angle at which a liquid-gas interface touches a solid surface. When a droplet of liquid is at rest on a solid surface, the contact angle only depends on the material properties of the liquid and the solid. In this thesis, the liquid phase discussed is water unless otherwise mentioned. As shown in Figure 1.5, if a water droplet is on a hydrophilic solid surface, water molecules spread and $\theta < 90^o$ is observed. On the other hand, if water droplet is on a hydrophobic solid surface, the contact angle will be in the range of 90^o to 180^o. Young's equation provides a quantitative description of wetting phenomena:[45]

$$\gamma_{air/solid} - \gamma_{liquid/solid} - \gamma_{air/liquid}\cos\theta = 0 \tag{1.7}$$

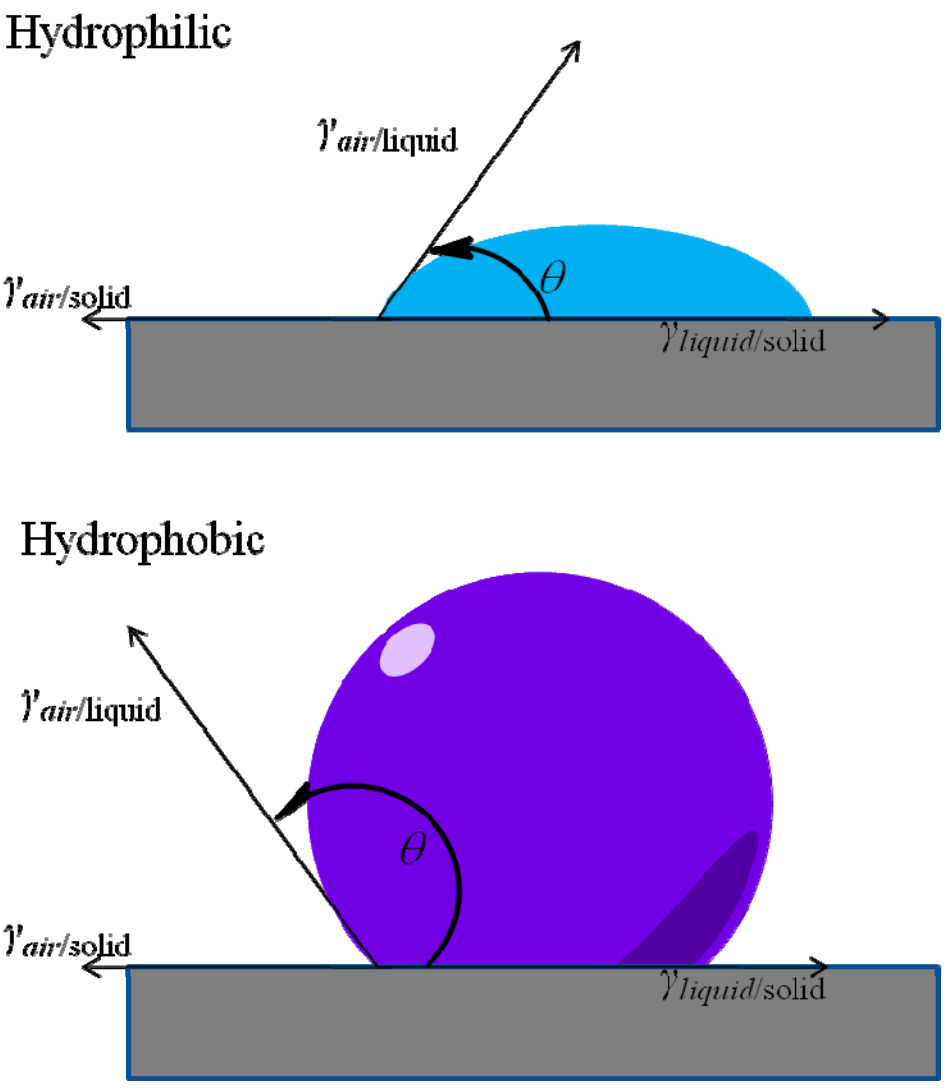

Figure 1.5 Contact angles of water on hydrophilic and hydrophobic surfaces.[46]

Paper or roughened plates often lead to perfect wetting ($\theta = 0^{o}$). Therefore, Equation 1.6 is sometimes written as:

$$\Pi = \gamma_0 - \gamma_{film} = \frac{F_{obs,0} - F_{obs,film}}{2L} \quad (1.8)$$

when t << L.

As seen in Equation 1.8, the surface pressure is the difference in surface tension between a clean or pure liquid (water) surface and a film covered surface. Π as a function of molecular (or monomer) area (*A*) at constant temperature is called a Π–*A* isotherm. Π-*A* isotherms are two-dimensional analogs of three dimensional pressure versus molar volume isotherms. Conceptually, A is nothing more than

$$A = \frac{A_{trough}}{N} \quad (1.9)$$

where A_{trough} is the area of the trough and *N* is the number of molecules on the surface. *A* and *N* are easily calculated by knowing A_{trough}, the concentration of the spreading solvent and the amount of spreading solution spread. Phase changes may be identified by monitoring Π as a function of *A*.

When *A* (Figure 1.6) is very large, molecules are far apart from each other; therefore the interactions between adjacent molecules are very weak. At this point, the amphiphilic molecules exist in a phase similar to a gas (G). As the molecules are compressed, the molecules will start to interact with each other and repulsive interactions will cause the molecules to start rising off the surface. As a consequence of the compression, liquid-expanded (LE) and condensed (LC) phases can form. A key difference between liquid phases is their densities. While condensed phases have densities that are similar to bulk liquids and solids, LE phases have densities that are ~ 50% smaller than 3D liquids. The other major difference is long-range order. For the LE phase, the

orientation of molecules is random. In contrast, traditional LC phases for molecules structurally similar to fatty acids are a collection of ordered phases with different tilt angles and unique packing which can be differentiated in grazing incidence X-ray diffraction (GIXRD) studies.[47] Prior to monolayer formation, LE and the LC phases can coexist with G to form G/LE or G/LC coexistent phases at $\Pi \sim 0$.[48]

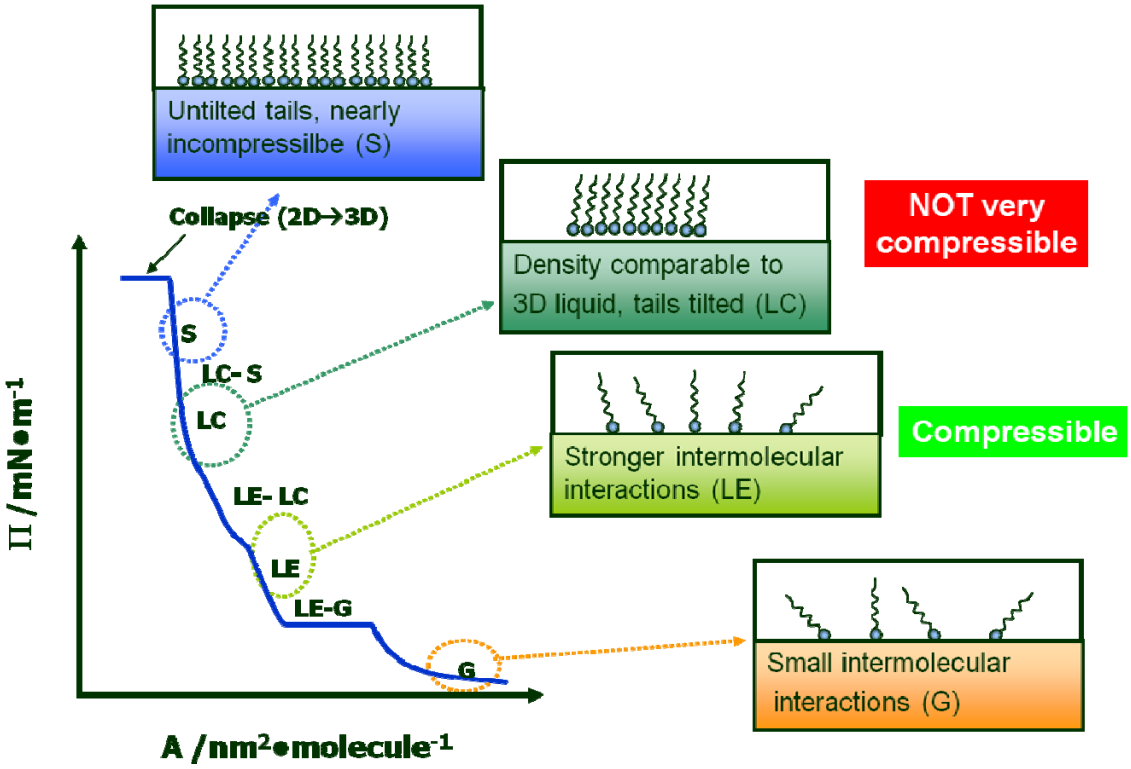

Figure 1.6 A schematic depiction of a Π-*A* isotherm for amphiphilic molecules at the A/W interface. The area scale on the plot roughly corresponds to room temperature values for fatty acids, where A_0 for the condensed phase is in the vicinity of 20 $Å^2 \cdot molecule^{-1}$.[47a]

Figure 1.6 is idealized. A film need not exhibit both an LE and LC or solid (S) phases. Special molecules like stearylamine (deposited on water acidified to pH=2.5 with HCl),[49] addition of

Cu^{+2} to 4-(((10,12-pentacosadiynoyl)oxy)methyl)pyridine,[50] amino-acid-derivatized diacetylene lipid,[51] *n*-octadecyltrichlorosilane (OTS),[52] phospholipid,[53] poly(l-lactic acid) (PLLA),[54] form both LE and LC phases. For these systems there is a first order phase transition between the LE and LC phases leading to phase coexistence.[55] As already noted, GIXRD studies showed the traditional LC phase was actually a collection of different phases that could be distinguished on the basis of their long-range order and average tilt angles. For example, fatty acids are known to form up to 9 condensed phases.[56] One of these is the solid phase (S), where the tilt angle is zero. Transitions between other LC phases and S are manifested as kinks rather than plateaus and tend to be second-order transitions.[57] At sufficiently high Π, all monolayers undergo collapse transitions.[48] Whether this transition entails the formation of multilayer structures (Figure 1.7) or dissolution into the bulk subphase is dependent upon the molecular structure.

As noted in the previous paragraph, monolayer phase transitions can be either first-order (common phase transition from undergraduate thermodynamics) or second-order (much rarer).[57] In general, a transition for which the first derivative of the chemical potential with respect to temperature is discontinuous is classified as a first-order transition. As a result, the densities of the two phases are discontinuous and a plateau in the Π-*A* isotherm is observed. In contrast, for second-order transitions, the first derivative of the chemical potential with respect of temperature is continuous but the second derivative is discontinuous. As noted, G-LE, G-LC, and LE-LC phase transitions are first-order. However, Π-*A* isotherm studies may be ambiguous because of kinetic effects and the influence of line tension.[58] For example, the nature of the LE-LC transition of *n*-pentadecanoic acid was argued for years and scientists only reached agreement after BAM and fluorescence microscopy showed the nucleation and growth of the LC phase.[57]

As one may notice in Figure 1.6, at the end of solid phase, molecules are no longer compressible and after a so-called "collapse" transition 3D structures are formed as depicted in Figure 1.7 or dissolution of parts of the Langmuir film occurs. The surface pressure corresponding to collapse is defined as the "collapse pressure" ($\Pi_{collapse}$), which indicates the limit of the stability of a 2D monolayer. Normally, the value of $\Pi_{collapse}$ is related to the barrier speed (compression rate) and the history of the film. A schematic diagram (Figure 1.7) demonstrates the process of collapse. As seen in Figure 1.7, compression of amphiphilic molecules with a constant force after the formation of a stable 2D monolayer ultimately pushes some molecules out of the monolayer away from the water subphase. During the transition, the hydrophobic tails of the upper molecules will interact with hydrophobic tails of the molecules in the bottom layer. However, the exact multilayer structures depend upon specific materials with most molecules tending to form different multilayer structures.[59]

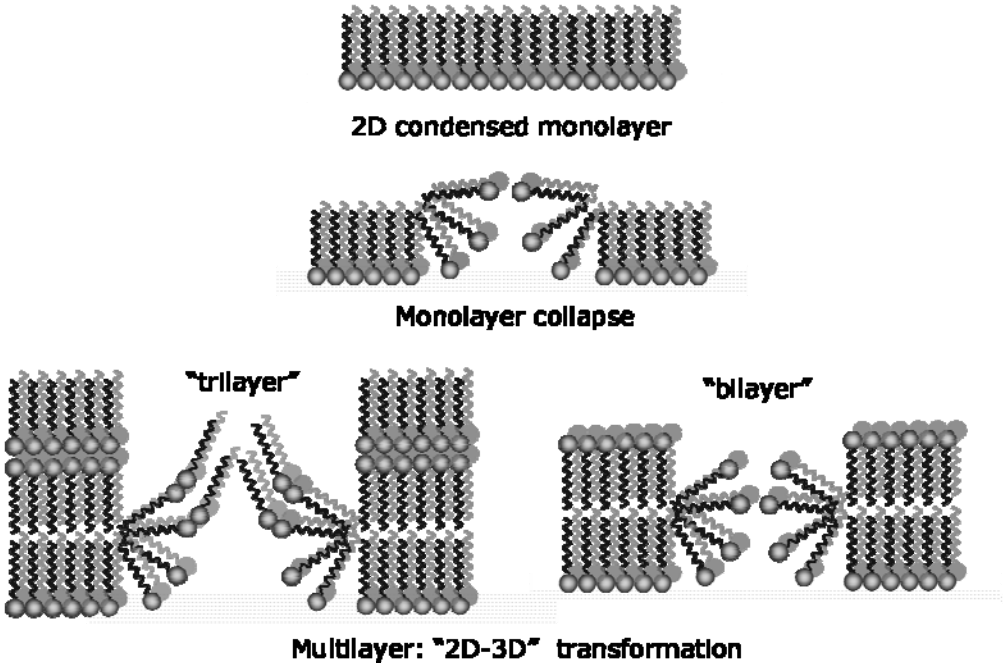

Figure 1.7 A schematic depiction of a Langmuir film undergoing collapse from a monolayer into multilayer domains.

An LB film contains one or more monolayers of a material deposited onto a solid substrate from a Langmuir film. An LB-film is formed by passing a solid substrate through the A/W interface of a Langmuir film. For special materials a monolayer is added with each immersion or emersion step, resulting in films with precisely controlled thicknesses. The procedures for preparing LB-films and measuring Π–*A* isotherms are similar.

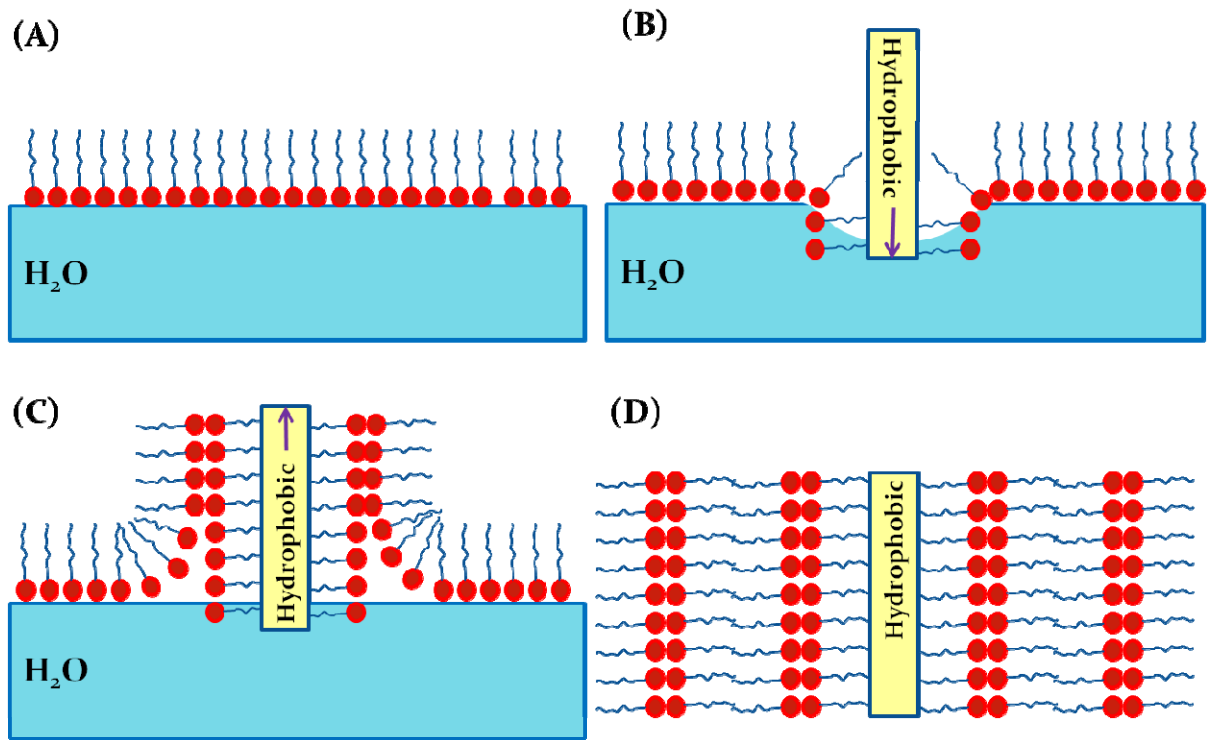

Figure 1.8 Y-type deposition of LB-multilayers onto a hydrophobic substrate: (A) formation of a stable Langmuir monolayer at the A/W interface by compression, (B) first immersion of a hydrophobic substrate, (C) first withdrawal, and (D) LB-multilayers with head-to-head and tail-to-tail configurations.[60]

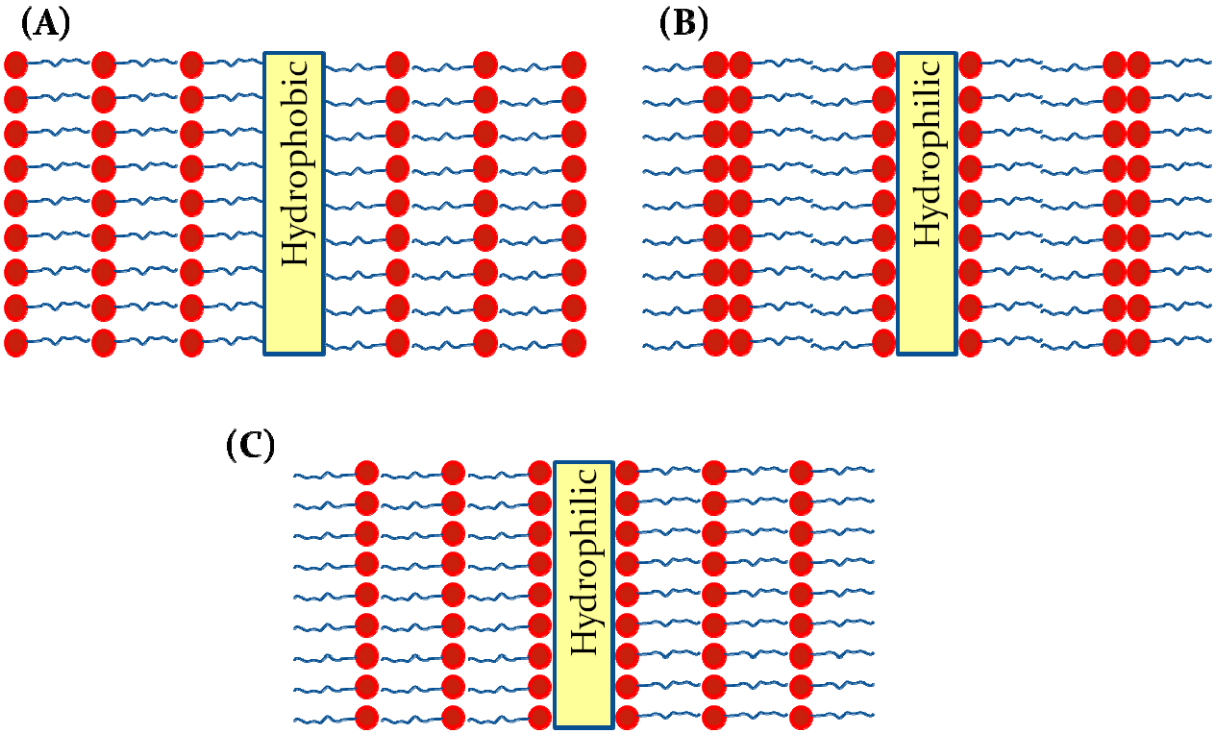

Figure 1.9 Structures of LB-multilayers: (A) X-, (B) Y-, and (C) Z-type. The structural difference between Figure 1.8 D and (B) reflects the fact that (B) depicts a hydrophilic substrate. X- and Z-type depositions do not normally guarantee that the multilayers will have the corresponding structure as rearrangement with time after deposition is possible.[61]

Several transfer modes for the deposition of molecules onto a substrate are depicted in Figures 1.8 and 1.9. For Y-type deposition onto a hydrophobic substrate (Figure 1.8), the substrate is lowered into the subphase and the molecules are oriented with their hydrophobic tail regions towards the substrate for the first layer. On the upstroke, the polar hydrophilic headgroups of the molecules on the surface are attracted to the outward facing headgroups that have already been deposited on the substrate. Continuous upstrokes and downstrokes can yield a multilayer LB-film. With an even number of layers, the hydrophobic tails face the air in the final

layer. For the less common types of transfer, X-type (Figure 1.9b) and Z-type (Figure 1.9c) deposition, molecules are only deposited on the downstroke or upstroke, respectively. In contrast to Y-type deposition where molecules are deposited into an alternating superstructure, X- and Z-type transfer yield mutilayer films where each molecule in every layer theoretically has the same orientation. X-ray diffraction studies of multilayers prepared via X-type deposition usually show that a bilayer structure exists. As such, molecules rearrange during or after transfer to form a more energetically favorable conformation.[40, 62] Normally, these conformations have hydrophobic tails of the final layer oriented toward air.

1.3.2 Brewster Angle Microscopy (BAM)

Π–*A* isotherms have limitations with respect to determining phases and phase transitions in Langmuir monolayers.[40] Therefore, BAM and fluorescence microscopy are usually used to visualize the domain formation and growth during phase transitions in Langmuir films. A fundamental difference between the two techniques is that BAM is label-free, whereas a fluorescence probe must be added to most systems to do fluorescence microscopy. As our group primarily uses BAM, I will discuss this technique further. In addition to the ability of BAM to study phase transitions, BAM can even reveal *in situ* morphological information about the texture and homogeneity of Langmuir films.[63]

When light passes through an interface between two media, some of the light will be reflected at the boundary while the remainder will be refracted. However, at a specific angle (Figure 1.10), *p*-polarized light is not reflected. This special incident angle is called Brewster's angle, θ_B, which is named after the Scottish physicist, David Brewster.

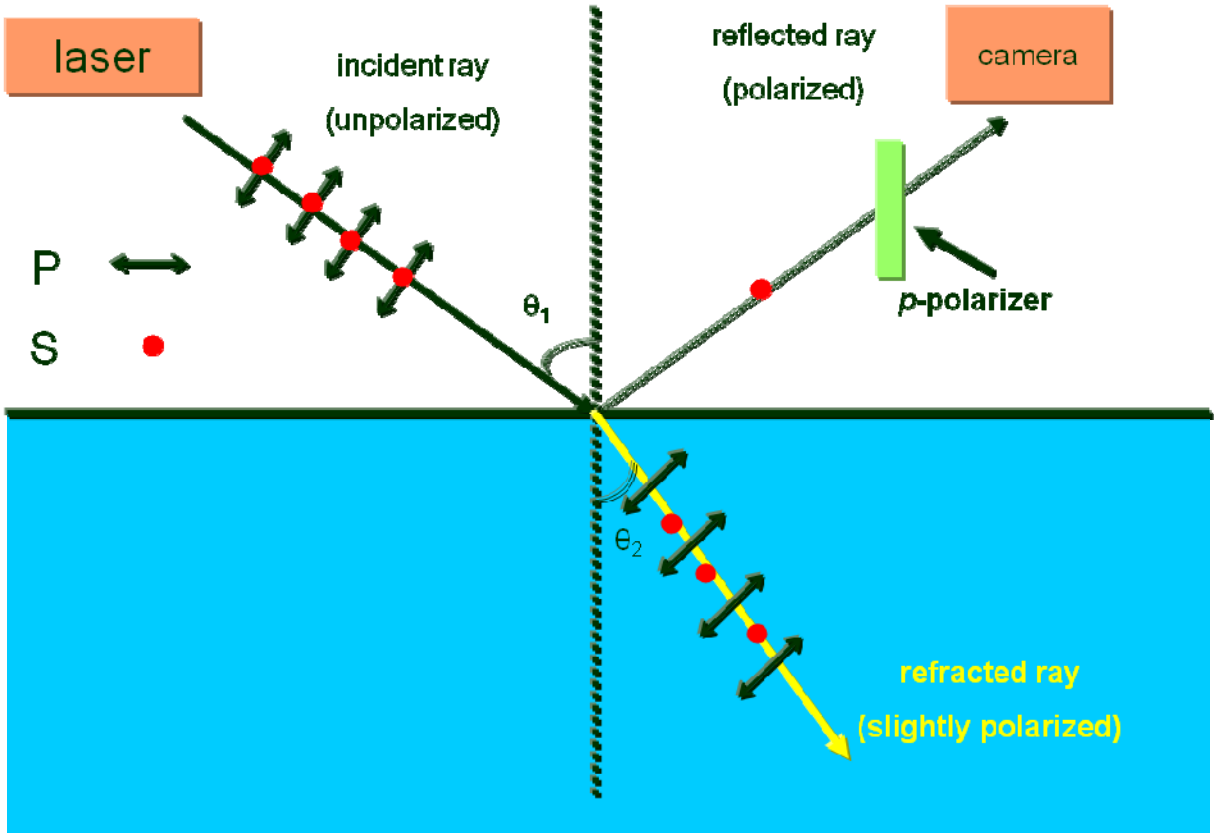

Figure 1.10 Schematic depiction of the reflection of unpolarized light at Brewster's angle.

Different components of linearly polarized light are defined according to their orientation relative to the plane of incidence (the surface of the paper in Figure 1.10). By convention, the electric field vector of *p*-polarized light is parallel to the plane of incidence, while the electric field vector of *s*-polarized light is perpendicular to the plane of incidence.[64] In Figure 1.10, P stands for *p*-polarized light and S represents *s*-polarized light. θ_1 is the angle of incidence and the angle of reflection, and θ_2 is the angle of refraction. Brewster's angle (θ_B) can be deduced from Snell's law:

$$n_1 \sin(\theta_1) = n_2 \sin(\theta_2) \tag{1.10}$$

where n_1 and n_2 are the refractive indices of medium *1* and *2*, respectively, and θ_1 and θ_2 are the angle of incidence and angle of refraction, respectively. At Brewster's angle, $\theta_1 + \theta_2 = 90°$. For the A/W interface, Brewster's angle corresponds to $\theta_1 = \theta_B = 53.1°$.

Brewster's angle can also be deduced from Fresnel's laws, which describe the reflectivity (R) of light as a function of incident angle and polarization. The reflectivity of *s*-polarized light (R_s) and *p*-polarized light (R_p) can be calculated from Equations 1.11 and 1.12, respectively:

$$R_s = \left(\frac{n_i \cos\theta_i - n_r \cos\theta_r}{n_i \cos\theta_r + n_r \cos\theta_i} \right)^2 = \frac{\sin^2(\theta_r - \theta_i)}{\sin^2(\theta_r + \theta_i)} \tag{1.11}$$

$$R_p = \left(\frac{n_r \cos\theta_i - n_i \cos\theta_r}{n_i \cos\theta_r + n_r \cos\theta_i} \right)^2 = \frac{\tan^2(\theta_i - \theta_r)}{\tan^2(\theta_r + \theta_i)} \tag{1.12}$$

where subscripts *i* and *r* represent incidence and refraction, respectively.

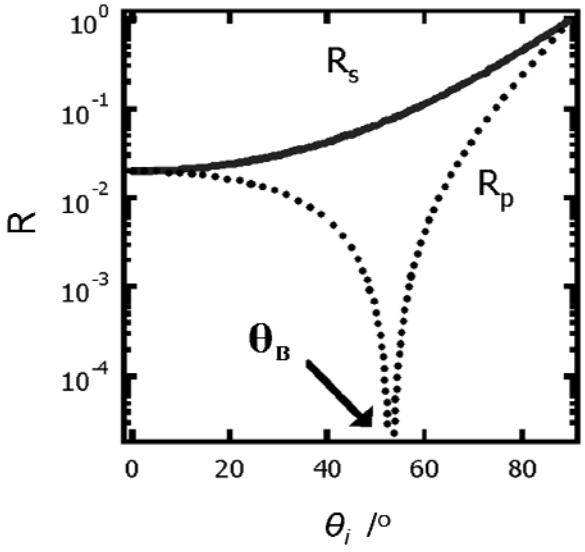

Figure 1.11 Reflectivity at different incident angles for S (solid line) and P (dotted line) polarized light.

For an ideal isotropic interface (Figure 1.11), R_s increases continuously with increasing incident angle while R_p exhibits a minimum, where the sum of θ_i and θ_r approach 90° causing $\tan(\theta_r + \theta_i) \rightarrow \infty$. For the case of Langmuir films where a sample is spread onto the surface of water, the thickness of the film and refractive index of the sample will cause some light to reflect at θ_B for the A/W interface. Under these conditions:[63a]

$$R_p(\theta_B) = R_s(\theta_B)\overline{\rho_B}^2 \tag{1.13}$$

where $R_p(\theta_B)$ and $R_s(\theta_B)$ represent the reflectivity of a Frensnel interface at Brewster's angle for *p*- and *s*-polarized light, respectively, and $\overline{\rho_B}$ is the average ellipticity at Brewster's angle which is defined as:

$$\overline{\rho_B} = \frac{\pi}{\lambda}\frac{\sqrt{n_2^2 + n_1^2}}{n_2^2 - n_1^2}\int_{-\infty}^{+\infty}\frac{[n(z)^2 - n_1^2][n(z)^2 - n_2^2]}{n(z)^2}dz \tag{1.14}$$

where λ is the wavelength of the incident light, and z within the integral indicates the distance from the average interfacial position, $z = 0$. If we can make the approximation that the thin film has a refractive index profile $n(z)$ that is uniform, the reflected intensity (I_r), at Brewster's angle will be proportional to the square of film thickness, h^2:

$$I_r = I_i R_p(\theta_B) \propto \overline{\rho_B}^2 \approx \left[\pi\frac{h}{\lambda}\frac{\sqrt{n_2^2 + n_1^2}}{n_2^2 - n_1^2}\frac{[n^2 - n_1^2][n^2 - n_2^2]}{n^2}\right]^2 \tag{1.15}$$

For any particular system, like the A/W interface, n_1 and n_2 are constants. Therefore, the thickness of the film can be obtained.

Figure 1.12 is a schematic depiction of a BAM with a laser source, a Glan-Thompson polarizer with the electric field vector parallel to the plane of incidence, and a light detector (such as a charge coupled device (CCD) camera). Since the light source is required to have a high intensity and a well defined polarization (*p*) for uniform illumination, a laser is the only reasonable choice. A polarizer is a device that converts a beam of light (electronic waves) of undefined or mixed polarization into a beam with well-defined polarization. Depending on various applications, there are basically two types of polarizers: linear polarizers and circular polarizers. Linear polarizers can be further divided into two categories: absorptive polarizers, where the filtered polarization states are absorbed and beam-splitting polarizers, where the unpolarized beam is split into two beams with opposite polarization states. Beam splitting polarizers are used for BAM. In traditional BAM, the polarizer is placed in the path of the incident beam to polarize the radiation in the *p* direction before it meets the surface. As the technique developed, the polarizer was moved to the path of the reflected beam to remove residual *s*-component before any reflected *p*-radiation reaches the CCD detector. This approach was found to enhance resolution.

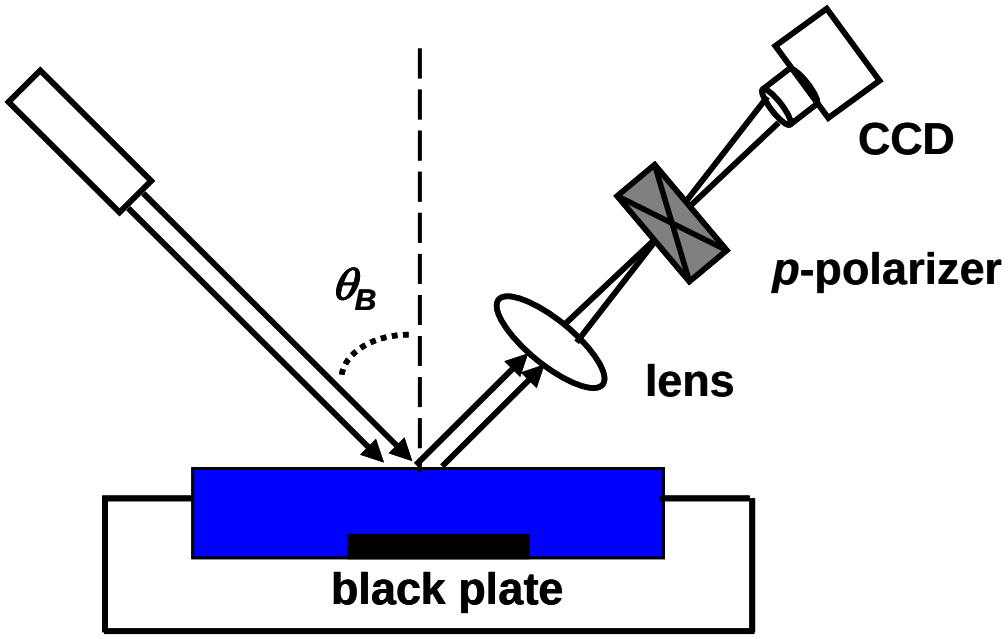

Figure 1.12 Schematic depiction of a BAM. A *p*-polarized laser beam is incident on the water surface at Brewster's angle for water (θ_B = 53.1°). Light reflected by the interface is detected by a CCD camera. A *p*-polarizer is placed in the path of the reflected beam to remove residual s-polarized light.

In the experiment, a tilted black glass plate is used underneath the water surface to prevent the light from randomly scattering from the subphase and trough. A set of lenses is used to direct the reflected beam to a CCD camera for imaging. Theoretically, nothing can be observed on the monitor when no film is present at the interface because *p*-polarized light is not reflected at Brewster's angle, while *s*-polarized light is blocked by the *p*-polarizer. However, once a sample is spread onto the A/W interface, Brewster's angle changes as the refractive index of the sample differs from water. Thus, even a trivial alteration results in some reflected *p*-polarized light reaching the CCD camera. Therefore, BAM is widely considered as a sensitive instrument for

detecting and studying phase transitions, phase separation, crystallization, aggregation, etc, when it is coupled with Π-*A* isotherms.[65]

Chapter 2

Experimental Materials and Methods

2.1 Materials and Sample Preparation

2.1.1 Obtained Materials

The reagents and solvents noted in this section were used for the synthesis and characterization of the polyhedral oligomeric silsesquioxane (POSS) derivatives from PSS-(3-hydroxypropyl)-heptaisobuyl (POSS-OH) described in this thesis. PSS-(3-hydroxypropyl)-heptaisobuyl (FW 875.30, mp 233.0-234.1 ºC) from the Aldrich Chemical Co. was purified by flash chromatography. All other reagents were used without further purification. Weisocyanate was purchased from Frontier Scientific, Inc. Triethylamine (TEA, reagent, ACS grade, FW 101.12 g/mol) and trifluoroacetic acid (TFA, reagent, ACS grade, FW 114.02 g/mol) were purchased from Aldrich Chemical Co. as a catalyst and reagent, respectively. Chloroform ($CHCl_3$, reagent, 99%, ACS grade, FW 119.38 g/mol), hexanes (reagent, 99%, ACS grade, FW 86.18 g/mol), ethyl acetate (EtOAc, reagent, 99%, ACS grade, FW 88.11 g/mol), methanol (MeOH, reagent, 99%, ACS grade, FW 32.04 g/mol) were purchased from Aldrich Chemical Co. as solvents. Poly (*tert*-butyl acrylate) (PtBA, number average molar mass M_n = 5500 $g \cdot mol^{-1}$, and polydispersity index M_w/M_n = 1.07) was purchased from Polymer Source, Inc. Trisilanolisobutyl-POSS (TiBP) was produced from Hybrid Plastics, Inc. and was used as received. Spreading solutions were prepared with nominal concentrations of around 0.5 $mg \cdot mL^{-1}$

in HPLC grade chloroform. All aqueous subphases were prepared from ultrapure water (Milli-Q Gradient A-10, 18.2 MΩ·cm, < 10 ppb organic impurities).

2.1.2 Purified and Synthesized Materials

2.1.2.1 Purification and Characterization of POSS-OH

From 206 mg of commercial POSS-OH (**1**, in Figure 2.1), was isolated as a crystalline white solid (195 mg, 94.7%) from a silica gel (60 Å) column by using methanol/ethyl acetate/ and hexane (10/10/80) as the eluant, and characterized: mp 233.0-234.1 °C; ^{1}H NMR (500 MHz, $CDCl_3$) δ 3.61 (q, J = 6.5 Hz, 2H), 1.88-1.80 (m, 7H), 1.69-1.63 (m, 2H), 1.33 (t, J = 5.5 Hz, 1H), 0.94 (d, J = 6.5 Hz, 42H), 0.64-0.58 (m, 16H); ^{13}C NMR (125 MHz, $CDCl_3$) δ 65.1, 26.1, 25.8, 24.0, 22.5; ^{29}Si NMR (82 MHz, $CDCl_3$) δ -66.8, -67.1, -67.4; HRMS calcd for $C_{31}H_{71}O_{13}Si_8$ $(M+H)^+$ 875.3043, found 875.3065; IR υ (cm^{-1}) 3405, 1081; Anal. Calcd for $C_{31}H_{70}O_{13}Si_8$: C, 42.52; H, 8.06. Found: C, 42.49; H, 8.16.

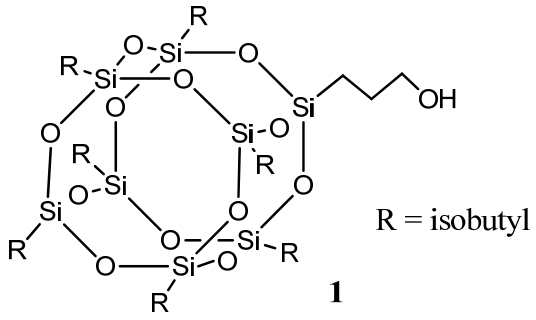

1

Figure 2.1 Structure of POSS-OH

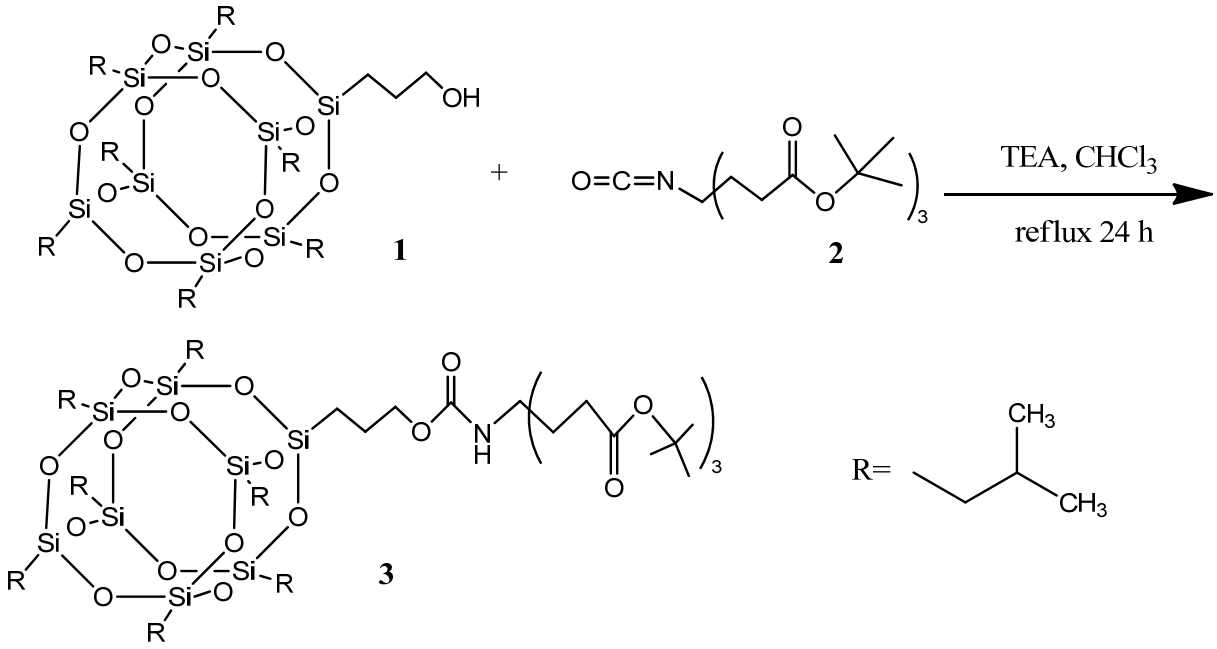

Scheme 2.1 Synthesis of POSS-triester (**3**)

2.1.2.2 Synthesis and Characterization of POSS-triester

Compound **1** (0.875 g, 1.0 mmol) and Weisocyante (**2**, 0.486 g, 1.1 mmol of) were dissolved in 3.0 mL of chloroform. Triethylamine (TEA) 1.0 mL was added to the solution dropwise. The reaction was stirred and refluxed for 24 hours. The solution was then removed under reduced pressure and the residue was separated by a silica gel (60 Å) column with ethyl acetate : hexane (15 : 85) yielding compound **3** (in Scheme 2.1) as a white solid (1.13 g, 85.8%): mp 101.3-102.7 °C; ^{1}H NMR (500 MHz, $CDCl_3$) δ 4.69 (s, 1H), 3.92 (t, *J* = 5.5 Hz, 2H), 2.21 (t, *J* = 8.0 Hz, 6H), 1.91-1.82 (m, 13H), 1.69-1.63 (m, 2H), 1.43 (s, 27H), 0.95 (d, *J* = 6.5 Hz, 21H), 0.94 (d, *J* = 6.5 Hz, 21H), 0.61-0.58 (m, 16H); ^{13}C NMR (125 MHz, $CDCl_3$) δ 172.7, 80.6, 66.5, 56.4, 30.2, 30.0, 28.2, 25.8, 23.9, 22.5, 8.3; ^{29}Si NMR (82 MHz, $CDCl_3$) δ -67.1, -67.2, -67.4; HRMS calcd

for $C_{54}H_{109}NO_{20}Si_8Na$ $(M+Na)^+$ 1338.5589, found 1338.5608; IR υ (cm^{-1}) 3369, 1728, 1095; Anal. Calcd for $C_{54}H_{109}NO_{20}Si_8$: C, 49.24; H, 8.34; N, 1.06. Found: C, 49.02; H, 8.41; N, 1.06.

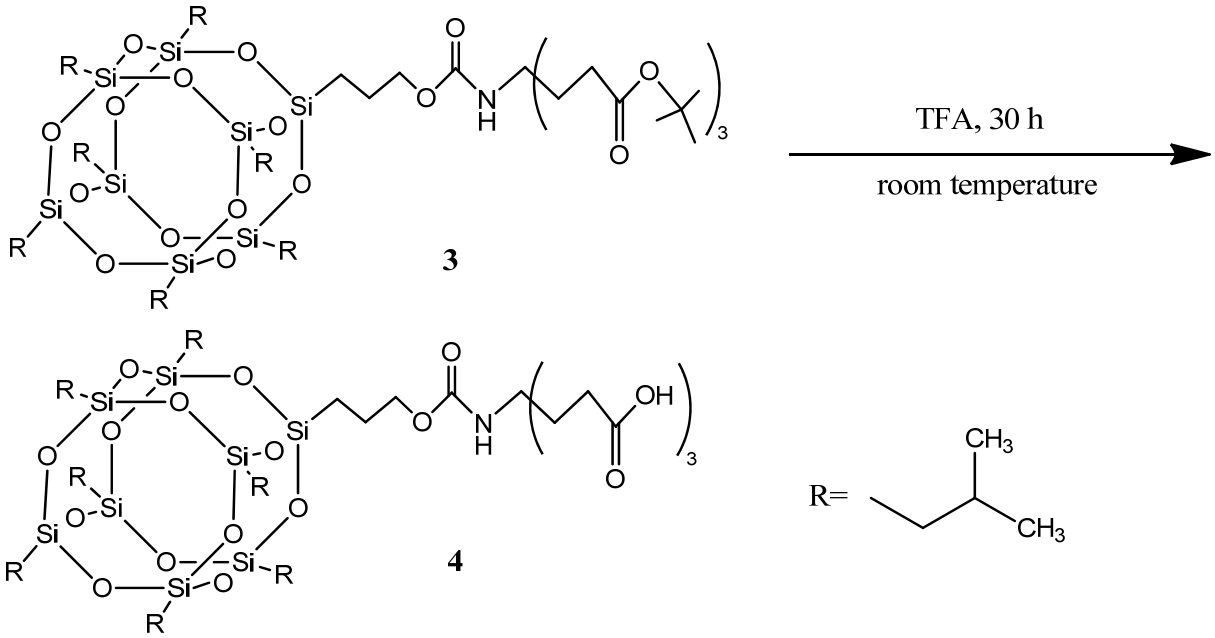

Scheme 2.2 Synthesis of POSS-triacid (**4**)

2.1.2.3 Synthesis and Characterization of POSS-triacid

Compound **3** (0.395g, 0.3 mmol) was added to TFA (4.0 mL) in a 50 mL round bottom flask. The reaction was stirred at room temperature for 30 hours. Then, the solvent was removed under reduced pressure and the residue was washed with dichloromethane (3 × 10 mL) as a chase solvent under reduced pressure. After drying overnight under vacuum, a white compound **4** (in Scheme 2.2) was obtained (0.318 g, 92.4%) and characterized: mp 178.0-179.1°C; ^{1}H NMR (500 MHz, $CDCl_3$) δ 4.49 (s, 1H), 3.95 (br t, 2H), 2.37 (br t, 6H), 1.97 (br t, 6H), 1.89-1.80 (m, 7H), 1.68 (m, 2H), 0.95 (d, J = 6.5 Hz, 42H), 0.62-0.59 (m, 16H); ^{29}Si NMR (82 MHz, $CDCl_3$) δ

-67.1, -67.4; HRMS calcd for $C_{42}H_{86}NO_{20}Si_8$ $(M+H)^+$ 1148.3892, found 1148.3914; IR υ (cm^{-1}) 3300, 1712, 1094; Anal. Calcd for $C_{42}H_{85}NO_{20}Si_8$: C, 43.91; H, 7.46; N, 1.22. Found: C, 43.87; H, 7.56; N, 1.13.

2.1.3 Prepared Solutions

pH controlled solutions were also used in this thesis:

(A) A pH = 8 solution was made from 1:1:1 mixtures by volume of 20 mM Trizma base: 100 mM NaCl : 2 mM $CaCl_2$. The resulting solution (pH ~ 9.8) was adjusted to pH = 8 by adding concentrated HCl dropwise.

(B) A 2.5 mM sodium tetraborate solution afforded pH = 9.1 and was used as made.

(C) Approximately pH = 11 and 13 solutions were made from 0.001 M and 0.1 M NaOH solutions, respectively.

Specific pH values were measured with an accumet® Basic AB15/15+ pH meter.

2.2 Sample Characterization

2.2.1 Nuclear Magnetic Resonance (NMR) Spectroscopy

^{1}H NMR spectra were obtained with a JOEL Eclipse+ spectrometer operating at 500 MHz with a 45° pulse angle, acquisition time of 3.6 s and a 1 s relaxation delay with 32 scans. Samples were dissolved in $CDCl_3$ at a typical concentration of 0.05 to 0.1 g/mL). ^{13}C NMR spectra were obtained in $CDCl_3$ on a JOEL Eclipse+ spectrometer operating at 125 MHz with a

45° pulse angle, acquisition time of 1.0 s and a 1 s relaxation delay with 25000 scans. Since POSS materials contain silicon in the cage structure, ^{29}Si was also applied to confirm the structures of the synthesized compounds. The spectra were obtained with a JOEL Eclipse+ spectrometer operating at 82 MHz with a 45° pulse angle, acquisition time of 1.1 s and a 10 s relaxation delay with 20000 scans. Abbreviations used in the splitting pattern were as follows: s = singlet, d = doublet, t = triplet, q = quartet, quin = quintet, m = multiplet, and br = broad.

2.2.2 Fourier Transform Infrared Spectroscopy (FTIR)

Measurements in this thesis were conducted on a Nicolet Impact 400 FTIR spectrometer. IR spectra were recorded on neat samples with an FTIR equipped with a diamond attenuated total reflection system, and reported in cm^{-1}. The resolution of the spectra was 2 cm^{-1} for 300 scans.

2.2.3 Melting Point Determinations

Melting points were determined in open capillary tubes and were uncorrected. Melting point data are reported as a range: the temperature at onset of melting and the temperature at which the sample was completely liquid and a meniscus was evident. Rough measurements were made at a rate of 5 ^{o}C/minute. Final measurements were made at a heating rate of 1 ^{o}C/minute. Three experiments with differences less than 0.5 ^{o}C were considered acceptable.

2.2.4 Elemental Analysis

In this thesis, all elemental analyses were performed by Atlantic Microlab; Atlanta, GA.

2.2.5 High Resolution Mass Spectrometry (HRMS)

In this thesis, all HRMS spectra were obtained with an Agilent 6220 Accurate-Mass TOF LC/MS in the Analytical Services Laboratory of the Chemistry Department at Virginia Tech.

2.3 Experimental Methods

2.3.1 Langmuir Trough Configuration

The experimental results presented in this thesis were conducted with a standard Langmuir trough (500 or 700 cm^2, Nima Technology, Ltd., 601 BAM or 702 BAM, respectively) equipped with a BAM (MicroBAM3, NanoFilm Technologie, Ltd., lateral resolution of 8 μm). The instruments were housed in a Plexiglas™ box at 70 to 75% relative humidity and a dust free environment. The instruments are (Langmuir trough, BAM, and Plexiglas box) rested on a floating optical table to minimize stray light and mechanical vibrations (Newport RS-2000 & I-2000). The Langmuir trough was made of hydrophobic Teflon® and was cleaned by dichloromethane or chloroform. The Langmuir trough is filled with ultrapure water. Two movable barriers, made of hydrophilic acetal resin polymer (Delrin®) were cleaned with propan-2-ol. In the experiments, barriers were used to sweep the water surface during the compression of the monolayer to vary the surface area symmetrically from both sides of the film (in Figure 2.1).

The hydrophobic trough supported an approximately 1 mm brim of water above the top of the trough edge.

After the trough was cleaned, it was filled with ultrapure water; the barriers were allowed to move toward each other thereby collecting dust and surface-active contaminations into the center of the trough. Next, the dust and surface-active contaminants were suctioned off by a clean pipette connected to a vacuum pump. The cleaning procedure was repeated several times until the surface tension in the opened and closed barrier positions matched the reported value for water and remained constant for at least 30 minutes. After spreading the organic solution (usually chloroform), 25 to 30 minutes was allowed before measurements to ensure complete evaporation of the spreading solvent. Surface pressure, Π, was recorded by the Wilhelmy plate technique to ± 0.1 $mN \bullet m^{-1}$ during all isotherm measurements.

As depicted in Figure 1.3, a piece of completely wetted filter paper was used as the Wilhelmy plate to detect the surface pressure. In this thesis, the aqueous subphase is ultrapure water unless otherwise mentioned. The temperature of the subphase was usually maintained at 22.5 ^{o}C by circulating water from a water bath (Neslab RTE-111) through the base of the trough. Π-*A* isotherms were obtained automatically by a computer, which controlled the barrier positions and provided a read-out of Π.

The relationship between the temperature of the circulating water and the actual temperatures of the water subphase at various positions for the 702 BAM trough indicated that the actual temperature of the subphase at different positions differed from the temperature of the circulating water; however, the values at different trough positions were quite similar for a given temperature.[66] Hence, the reported temperature is the actual temperature of the subphase.

2.3.2 Constant Compression Rate Experiments

Constant compression rate experiments were used to obtain Π-*A* isotherms at compression rates of 10 $cm^2 \cdot min^{-1}$. The static elastic modulus, $\varepsilon_s = -A(\partial\Pi/\partial A)_T$, of the films were deduced from the recorded Π-*A* isotherms.

2.3.3 Brewster Angle Microscopy

BAM studies (MicroBAM3, NanoFilm Technologie, Ltd., lateral resolution of 8 μm) were carried out simultaneously during isotherm measurements, and BAM images were taken by a charge-coupled device (CCD) camera under the "automatic gain control" mode to obtain an optimal average brightness rather than absolute intensity values. The original size of all BAM images taken during the measurements was 3.6 × 4.8 mm^2, while some BAM images presented in this thesis with smaller sizes were cut from the original images utilizing imaging software.

Chapter 3

Characterization of POSS-Based Amphiphiles at the Air/Water Interface

3.1Abstract

A triester, polyhedral oligomeric silsesquioxane (POSS) derivative (POSS-triester) was synthesized from (3-hydroxypropyl)-heptaisobutyl-POSS (POSS-OH) and Weisocyanate. The resulting POSS-triester was converted into a triacid (POSS-triacid) with trifluroacetic acid. Surface pressure-area per molecule (Π-*A*) isotherm studies and Brewster angle microscopy (BAM) confirmed POSS-OH, POSS-triacid, and POSS-triester were amphiphilic at the air/water (A/W) interface. Analysis of the Π-*A* isotherms revealed packing of these amphiphiles at the A/W interface was significantly different from previously reported POSS amphiphiles. Whereas trisilanol-POSS derivatives pack in a vertex-on conformation, POSS-OH and POSS-triacid pack in a face-on conformation. For POSS-triester, there may be a transition from vertex-on to face-on packing during compression of the molecules at the A/W interface.

3.2 Introduction

Trisilanol polyhedral oligomeric silsesquioxane (POSS) derivatives have been studied and reported as a class of amphiphilic molecules that form stable Langmuir monolayers at the air/water (A/W) interface. Since these POSS manifested interesting phase transitions and aggregation behavior and were considered to be excellent model nanofillers with well defined sizes, the Esker group has systematically investigated these compounds.[33-34, 65e, 65g, 67] For

example, trisilanolphenyl-POSS (TPP) has been blended with poly(t-butyl acrylate) (PtBA) as a nanofiller. Although both the bulk and surface glass transition temperatures (T_g) increased as TPP was added to PtBA, the surface T_g increased more significantly with limited incorporation of the POSS component.[33] In another study, an open cage POSS, trisilanolisobutyl-POSS (TiBP), and a closed-cage POSS, octaisobutyl-POSS, were blended with poly(dimethylsiloxane) (PDMS) to compare their effects on PDMS films at the A/W interface.[67b] The amphiphilic trisilanol-POSS exhibited more interesting phase behavior than hydrophobic octafunctional POSS at the A/W interface because the closed-cage POSS was hydrophobic and aggregated.

In this chapter, purified (3-hydroxypropyl)-heptaisobutyl-POSS (POSS-OH) was added to Weisocyanate, in the presence of triethylamine (TEA),[68] and afforded a triester (POSS-triester), which was further converted into a triacid (POSS-triacid) by trifluoroacetic acid (TFA) (Schemes 2.1 and 2.2). As these POSS derivatives were amphiphilic, surface pressure-area per molecule (Π-*A*) isotherms and Brewster angle microscopy (BAM) were used to probe the quasi-two-dimensional thermodynamic and morphological properties of these materials, respectively, at the A/W interface. Differences in packing, as well as the effect of pH on the Π-*A* isotherms of POSS-triacid are discussed. The results indicate that POSS-triester is surface active forming liquid expanded (LE) monolayer while POSS-triacid forms liquid condensed (LC) films that are only weakly dependent on pH. Orientations of POSS derivatives at the A/W interface are proposed.

3.3 Experimental

Experimental details regarding the synthesis of POSS-triester (**3**) and POSS-triacid (**4**) are provided in Chapter 2.1.2.2 and 2.1.2.3, respectively. Experimental methods are covered in Chapter 2.3.

3.4 Synthesis and Characterization of POSS-triester and POSS-triacid

POSS-OH (**1 i**n Scheme 2.1) was insufficiently pure to begin the synthesis of POSS-triester (**3** in Scheme 2.1) and POSS-triacid (**4** in Scheme 2.2). Flash column separation was ultimately chosen for purification over recrystallization because it afforded better yields.

The synthesis of the novel dendritic amphiphilic molecules involved two steps (Scheme 2.1 and Scheme 2.2). In the first step, a slight molar excess of Weisocyanate (**2** in Scheme 2.1) reacted with POSS-OH (**1** in Scheme 2.1) with a molar ratio of **1**:**2** = 1:1.1 to 1:1.2. For the second step, 24 hours was deemed sufficient to completely hydrolyze POSS-triester since more than 30 hours leads to degradation of POSS-triester.

Chemical composition and purity were confirmed via ^{1}H NMR, ^{13}C NMR, ^{29}Si NMR, melting point, elemental analysis, FTIR, and HRMS. Figures 3.1, 3.3, and 3.5 contain the ^{1}H NMR spectra with melting point ranges for POSS-OH, POSS-triester and POSS-triacid in $CDCl_3$, respectively. Figures 3.2 and 3.4 contain the ^{13}C NMR spectra for POSS-OH, and POSS-triester in $CDCl_3$, respectively. The spectra reveal sharp, well-resolved peaks. The characteristic differences in the splitting pattern of the protons of the linker and essentially quantitative integrations were consistent with the labeled structures on each spectrum.

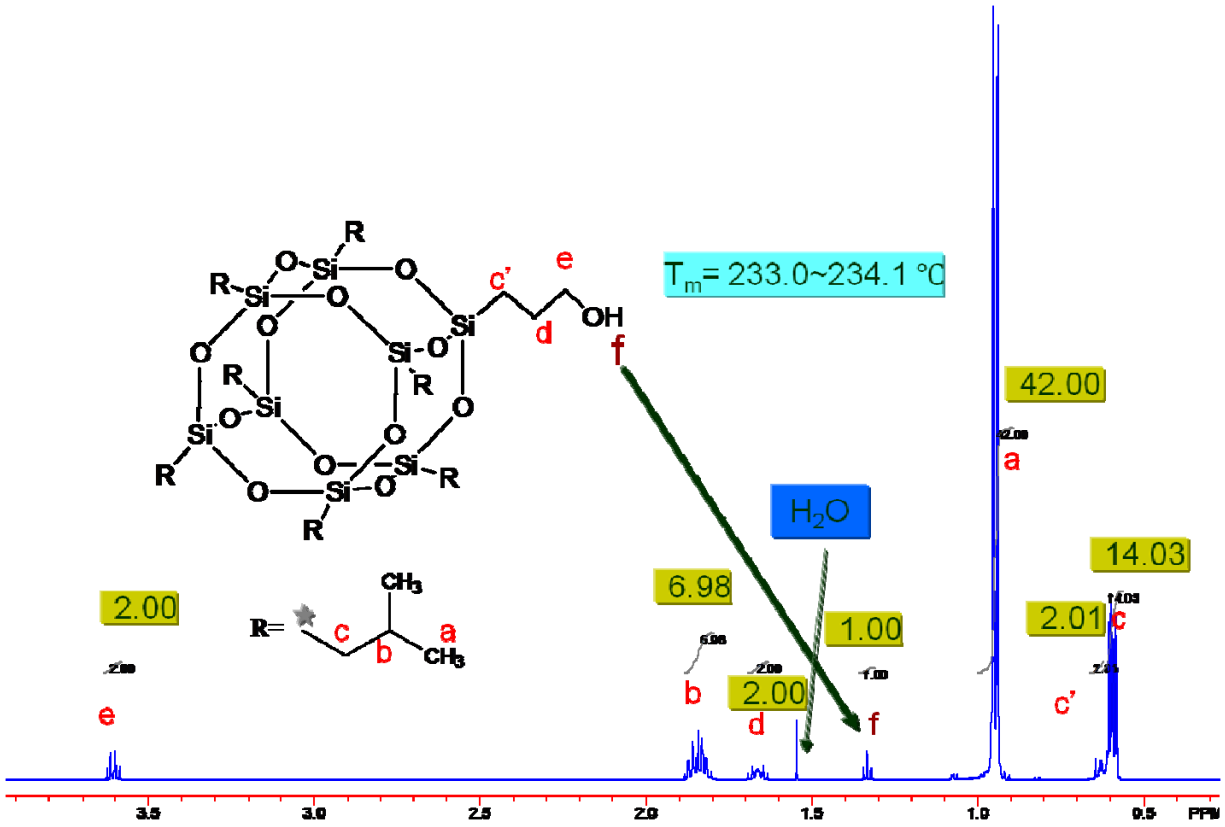

Figure 3.1 ^{1}H NMR and T_m of purified POSS-OH.

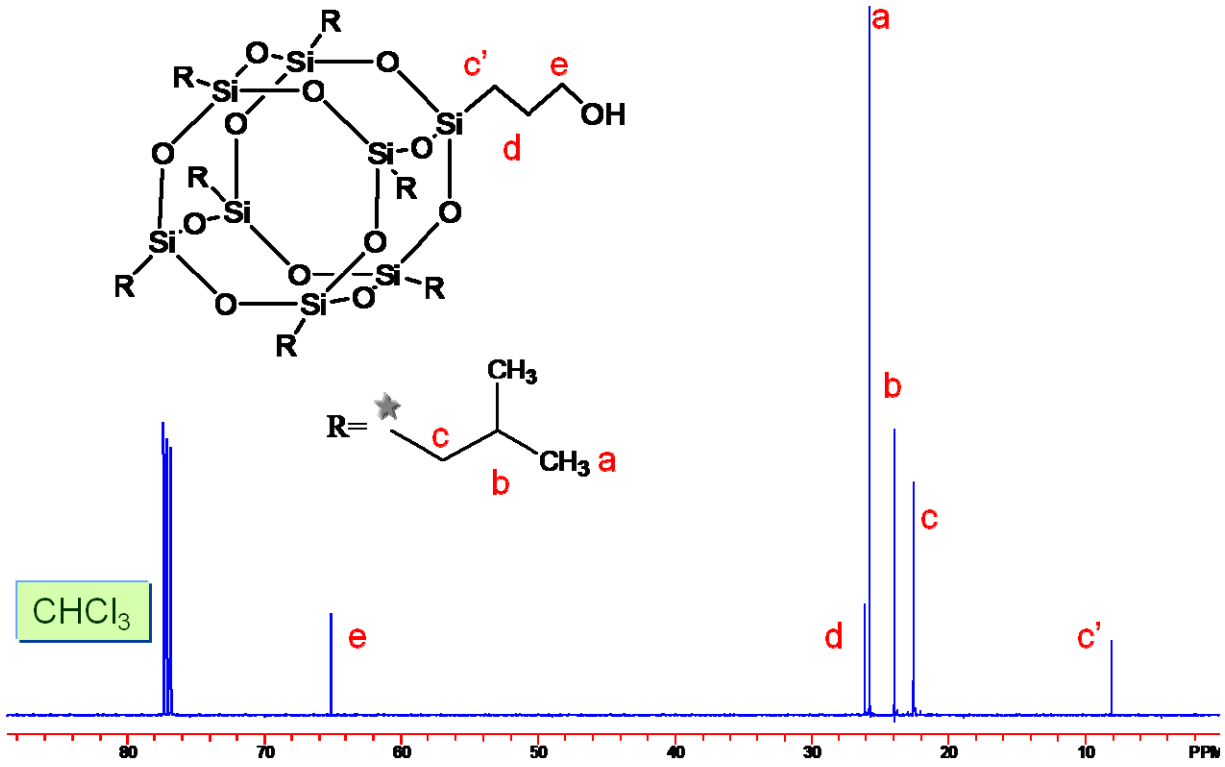

Figure 3.2 ^{13}C NMR of purified POSS-OH.

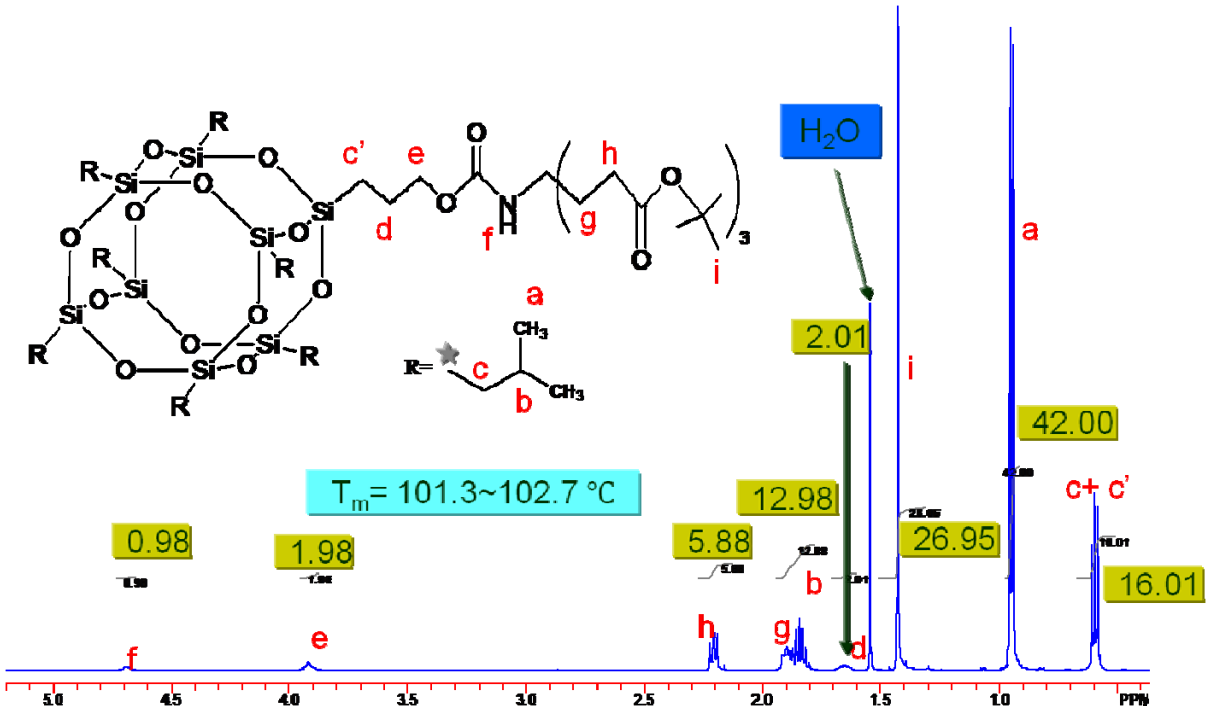

Figure 3.3 ^{1}H NMR and T_m of POSS-triester.

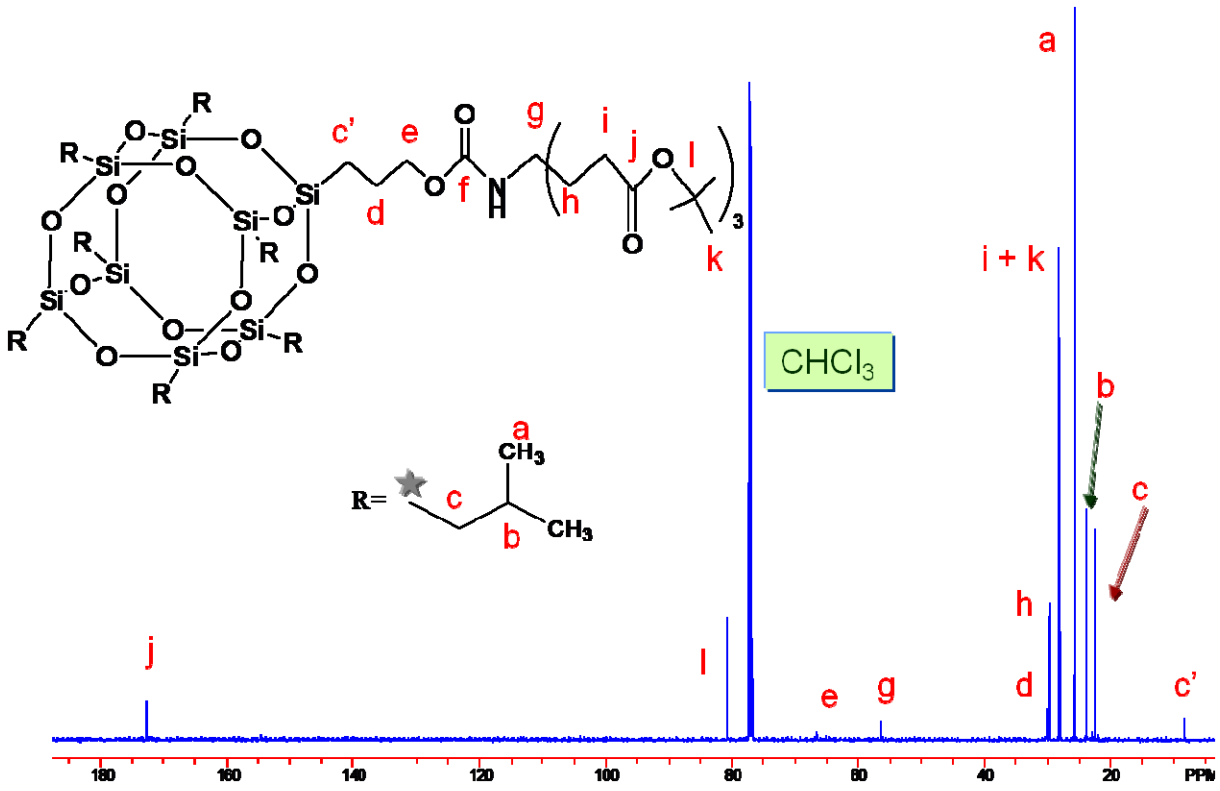

Figure 3.4 ^{13}C NMR of POSS-triester.

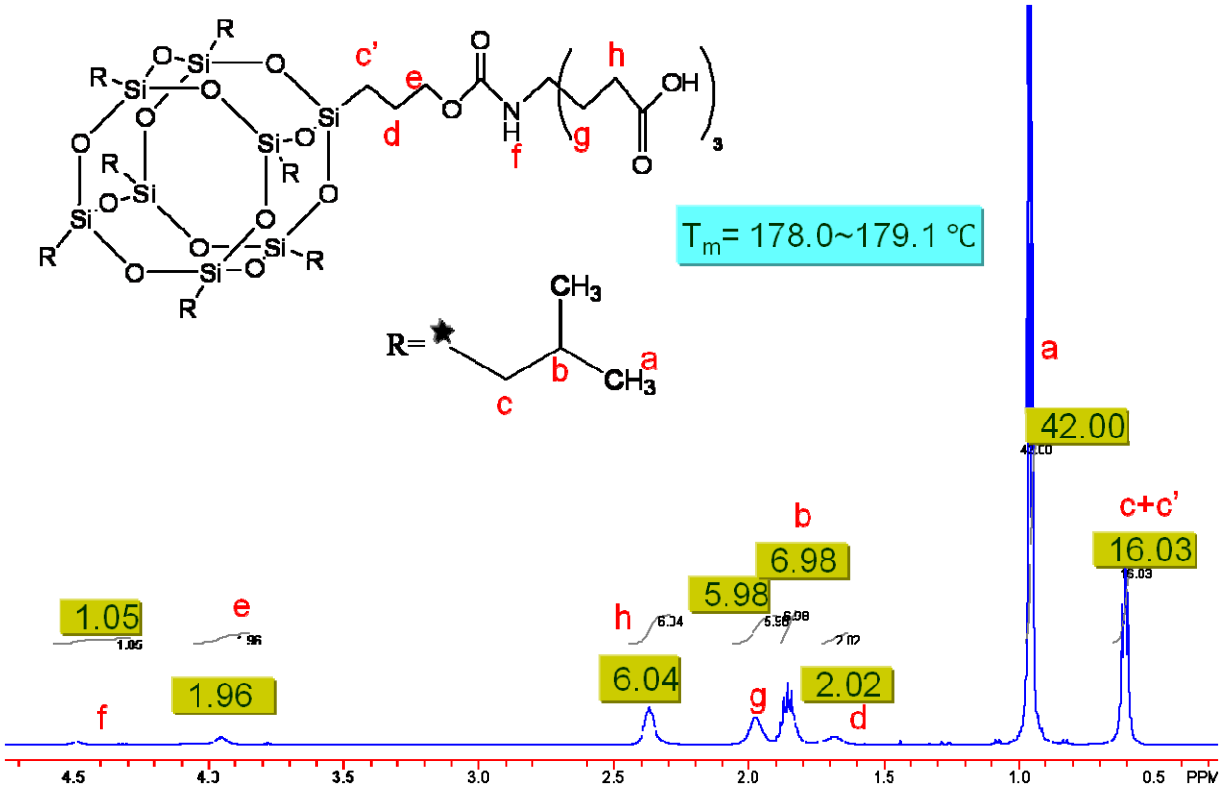

Figure 3.5 ^{1}H NMR and T_m of POSS-triacid.

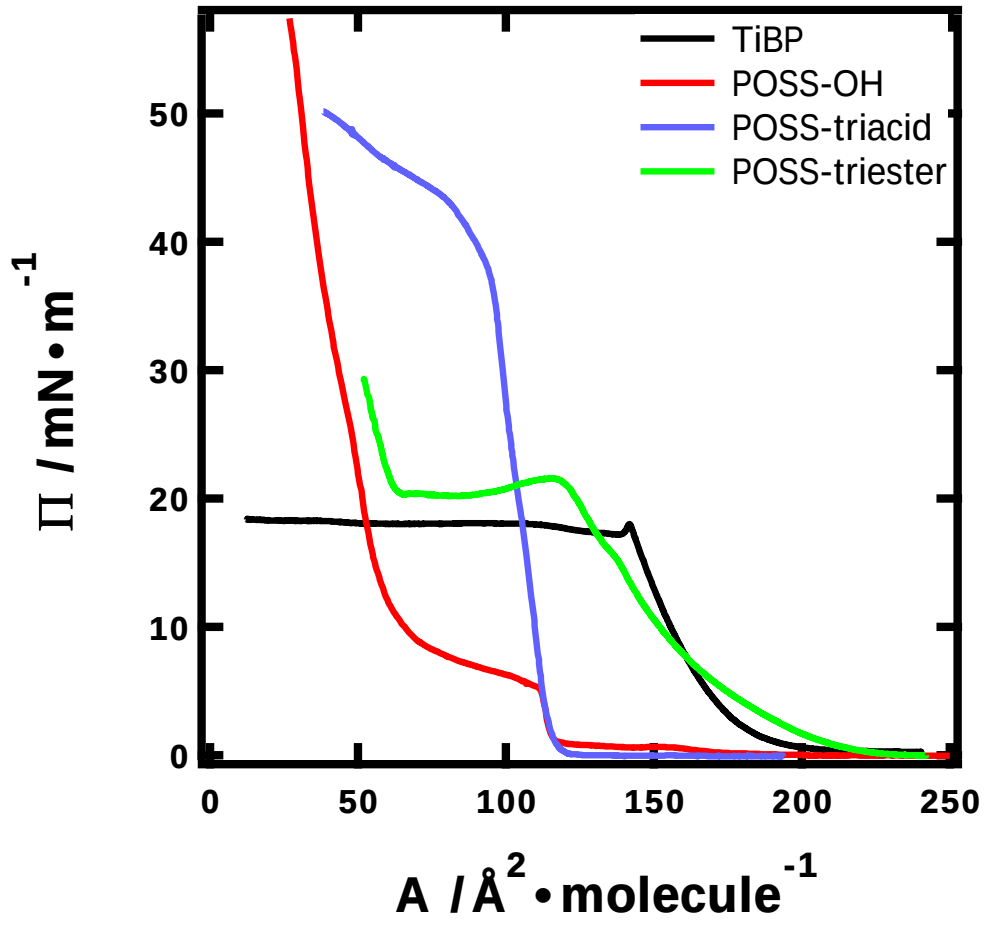

Figure 3.6 Π-*A* isotherms of trisilanolisobutyl-POSS (TiBP), POSS-OH, POSS-triacid, and POSS-triester at 22.5°C at the A/W interface.

3.5 Π-*A* isotherms of POSS-OH, POSS-triester, and POSS-triacid Langmuir Films

Figure 3.6 has Π-*A* isotherms for POSS-OH, POSS-triester, and POSS-triacid at the A/W interface at 22.5 °C. A Π-*A* isotherm for trisilanolisobutyl-POSS (TiBP)[65f] is also provided on Figure 3.6 as a reference. The Π-*A* isotherm for POSS-OH reveals a lift-off surface concentration ($A_{lift\text{-}off}$, where Π increases from zero) around $A_{lift\text{-}off}$ ~185 Å^2•molecule^{-1}, followed by a long

plateau until lower A (~ 125 Å^2•molecule^{-1}) at low Π (~ 1 mN•m^{-1}). This smaller A value corresponds to the limiting area (A_0), which was obtained by extrapolating the steepest portion of the Π-A isotherm back to Π = 0. At a relatively low collapse pressure (Π_c ~ 5 mN•m^{-1}), the POSS-OH film collapses into multilayer domains.

The second plateau (65 Å^2•molecule^{-1} < A < 110 Å^2•molecule^{-1}) corresponds to multilayer formation. The factor of two change in area may be consistent with bilayer formation. The long plateau at intermediate Π has also been observed for other weakly amphiphilic POSS derivatives, trisilanolcyclohexyl-POSS[65a] and trisilanolcyclopentyl-POSS.[69] At even smaller A, Π increases further as the multilayer structures are rigid.

For POSS-triacid, Π ≈ 0 until $A_{lift\text{-}off} = A_0$ = 125 Å^2•molecule^{-1}. The isotherm is similar to a classical long chain fatty acid or alcohol in that a nearly incompressible condensed (LC) phase forms with collapse of the film occurring at $A_c \approx$ 90 Å^2•molecule^{-1} and $\Pi_c \approx$ 40 mN•m^{-1}.

Moving onto POSS-triester, the isotherm is consistent with a more compressible monolayer. $A_{lift\text{-}off}$ ~215 Å^2•molecule^{-1} and A_0 ~175 Å^2•molecule^{-1} are much larger than POSS-OH and POSS-triacid. Moreover, the rise in Π in the monolayer regime (125 Å^2•molecule^{-1} < A < 215 Å^2•molecule^{-1}) is more gentle, like an LE monolayer. Collapse of the film at $A_c \approx$ 125 Å^2•molecule^{-1} and $\Pi_c \approx$ 22 mN•m^{-1} is followed by a plateau (65 Å^2•molecule^{-1} < A < 125 Å^2•molecule^{-1}) that is similar to POSS-OH. Further compression of the film (A < 65 Å^2•molecule^{-1}) also cause Π to increase like POSS-OH.

The other isotherm in Figure 3.6 is for trisilanolisobutyl-POSS (TiBP). Deng et al.[65e] interpreted this isotherm as follows:

$A > A_{lift\text{-}off}$ = 230 Å^2•molecule^{-1}: coexisting G/LE monolayer.

A_0 = 177 Å^2•molecule^{-1} < A < $A_{lift\text{-}off}$ = 230 Å^2•molecule^{-1}: LE monolayer.

A_c = 140 Å^2•molecule^{-1} < A < A_0 = 177 Å^2•molecule^{-1}: more condensed liquid-like monolayer.

A < A_c = 140 Å^2•molecule^{-1}: collapse into multilayer structures.

It is interesting to note similarities and differences between the isotherms in Figure 3.6. First, one would initially group POSS-OH and POSS-triacid together on the basis of a similar A_0 and note that this value is much smaller than TiBP. Second, the POSS-triester seems similar to TiBP with respect to $A_{lift\text{-}off}$ and A_0, however, A_c is similar to A_0 for POSS-OH and POSS-triacid.

As both A_0 and A_c serve as estimates of molecular cross-sections, and the cage portion of the molecules are the same (isobutyl substituents on seven silicon atoms), a natural question arises, "How are the POSS cages packing?" Before addressing this question, it is necessary to explore how electrostatic interactions associated with deprotonation of POSS-triacid influence isotherm.

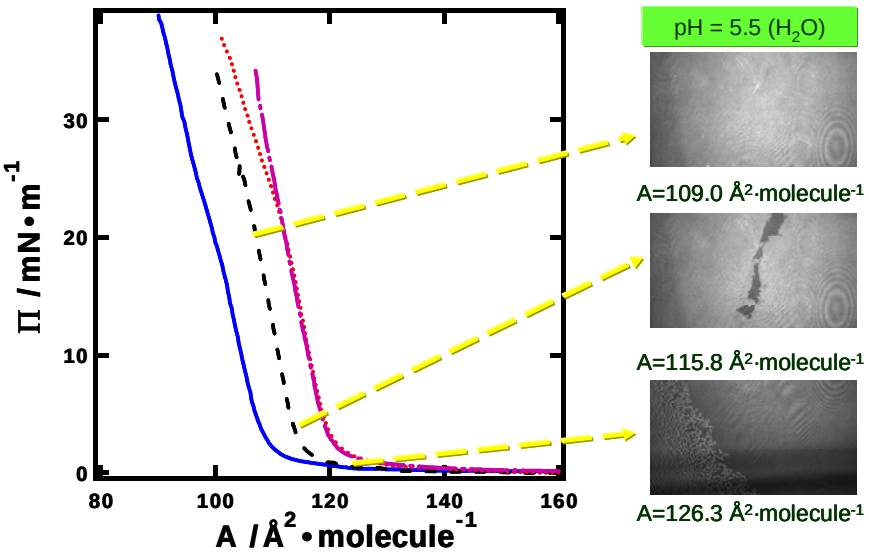

Figure 3.7 Π-*A* isotherms of POSS-triacid on subphases with different pH at T = 22.5 °C. The isotherms from left to right correspond to pH = 1.7 (—), 5.5 (- - -), 9.1 (···), and 11.4 (—·—). The 2.0 mm × 2.4 mm BAM images BAM images were captured with H_2O (pH = 5.5) as the subphase, at *A* = 126 (submonolayer), 116 (on-set of monolayer formation) and 109 (monolayer) $Å^2 \cdot molecule^{-1}$.

3.6 Isotherm and Morphology of POSS-triacid (4) on Different pH Subphases (T = 22.5 °C)

Figure 3.7 shows Π-*A* isotherms for POSS-triacid on subphases with different pH. As seen in Figure 3.7, decreasing pH relative to an ultrapure water subphase causes a shift in $A_{lift\text{-}off}$ to smaller *A*, whereas increasing pH relative to ultrapure water causes a shift in $A_{lift\text{-}off}$ to larger *A*. However, the shifts in *A* are small, < 5% and there are no other significant changes in the isotherms. Moreover, there is no change in the isotherm between pH= 9.1 and 11.4. From these observations, it appears that POSS-triacid is partially deprotonated at the A/W interface. This

result agrees with previous titration studies[70] of the tricarboxylato headgroup showing that the trianion dominates the equilibrium at pH ≥ 7. Additionally, a study[71] on the effect of pH on critical micelle concentration of tricarboxylato amphiphiles suggests that pH > 8 is required for complete ionization. Furthermore, the weak dependence of $A_{lift\text{-}off}$ on pH means that steric rather than electrostatic factors are primarily responsible for determining the effective size of the molecule in a close packed state at the A/W interface.

The other important information in Figure 3.7 is the BAM images. Heterogeneity in the representative BAM images obtained from films of POSS-triacid at pH = 5.5 prior to "monolayer" formation and in the "monolayer" are consistent with very rigid films. This feature is also reflected in the slope of the isotherms. The isotherms can be used to calculate static elastic moduli (ε_s = -A $(\partial\Pi/\partial A)_T$). Values of ε_s in excess of 200 $Å^2 \cdot molecule^{-1}$ for the isotherms in Figure 3.7 are consistent with very rigid LC films. These values of ε_s are well in excess of those reported for TiBP[65e] and suggest large differences in molecular packing exist between the molecules.

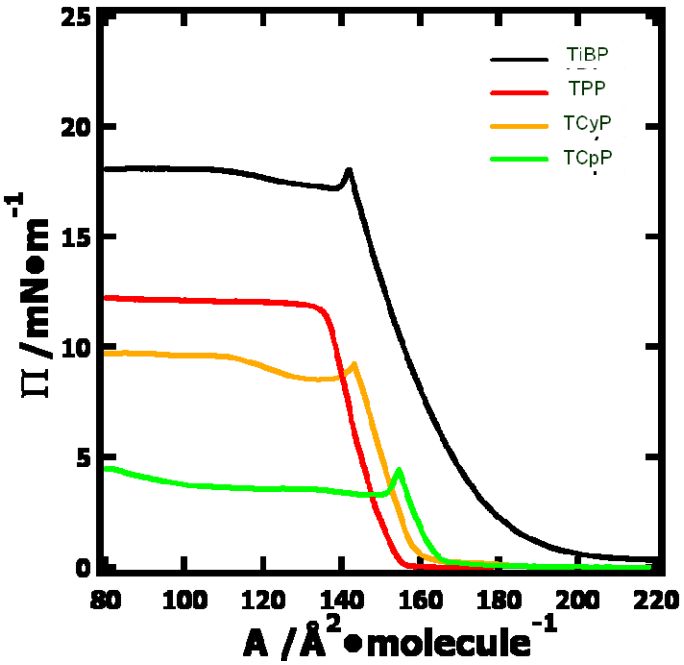

Figure 3.8 ∏-*A* isotherms for trisilanol-POSS derivatives. TiBP: trisilanolisobutyl-POSS; TPP: trisilanolphenyl-POSS; TCyP: trisilanolcyclohexyl-POSS; TCpP: trisilanolcyclopentyl-POSS.[69]

3.7 Proposed Conformations for POSS Cages in Langmuir Films

Traditional modeling of the structure of fatty acids in Langmuir films has treated the molecules as rod-like objects due to their large length/diameter ratio. As the length/diameter ratio decreases, the traditional amphiphiles become water-soluble leading to Gibbs monolayers (for fatty acids, C_{13} is the lower limit for the formation of insoluble monolayers).[24c] In contrast, the silsesquioxane core of POSS molecules is essentially a cube, while the flexible organic coronae have led to treatments of POSS as nanometer sized spheres. Hence the overall shape is essentially the same whether the POSS is a closed, eight silsesquioxane unit (T_8) cage or a seven unit (T_7) open cage trisilanol. One key difference is that the T_7 trisilanols exist as hydrogen

bonded dimers in the crystalline state.[24c] In order to obtain a thorough analysis of POSS molecules at the A/W interface, it is critical to master the orientations of molecules in a two-dimensional (2D) system. Π-*A* isotherms not only can reveal the quasi 2D thermodynamic properties, but also can yield A_c of a molecule from the limiting area (A_0). Previous studies with POSS have focused on trisilanol-POSS derivatives.[35a, b, 65a, 65e, 65g, 67b, 72] Figure 3.8 compares Π-*A* isotherms of a series of trisilanol-POSS and indicates that the A_0 of different POSS molecules are affected by their substituents, while A_c values exhibit less variance. For all the Π-*A* Isotherms, the smallest A_0 is > 150 $Å^2$•molecule^{-1}. Since all the compounds of interest in this thesis have isobutyl substituents, TiBP is the relevant reference compound for subsequent discussion.

According to Figure 3.8, the limiting area of TiBP is A_0 ~180 $Å^2$•molecule^{-1} corresponding to a closely packed state at the A/W interface. In order to understand the liquid-like state, TiBP was modeled with known crystal structure of TCyP[24c] and CS Chem Draw Pro to substitute isobutyl groups for cyclohexyl groups on the cage. In Chem Draw 3D, MM2 and MOPAC calculations in vacuum were run to minimize the energy state of the structures. Finally, a barrel-like model and a cross-sectional area of 177 $Å^2$•molecule^{-1} were suggested for TiBP.[65e] In this model, the silsesquioxane core had a vertex-on conformation at the A/W interface. Further insight into this conformation is provided in the subsequent discussion.

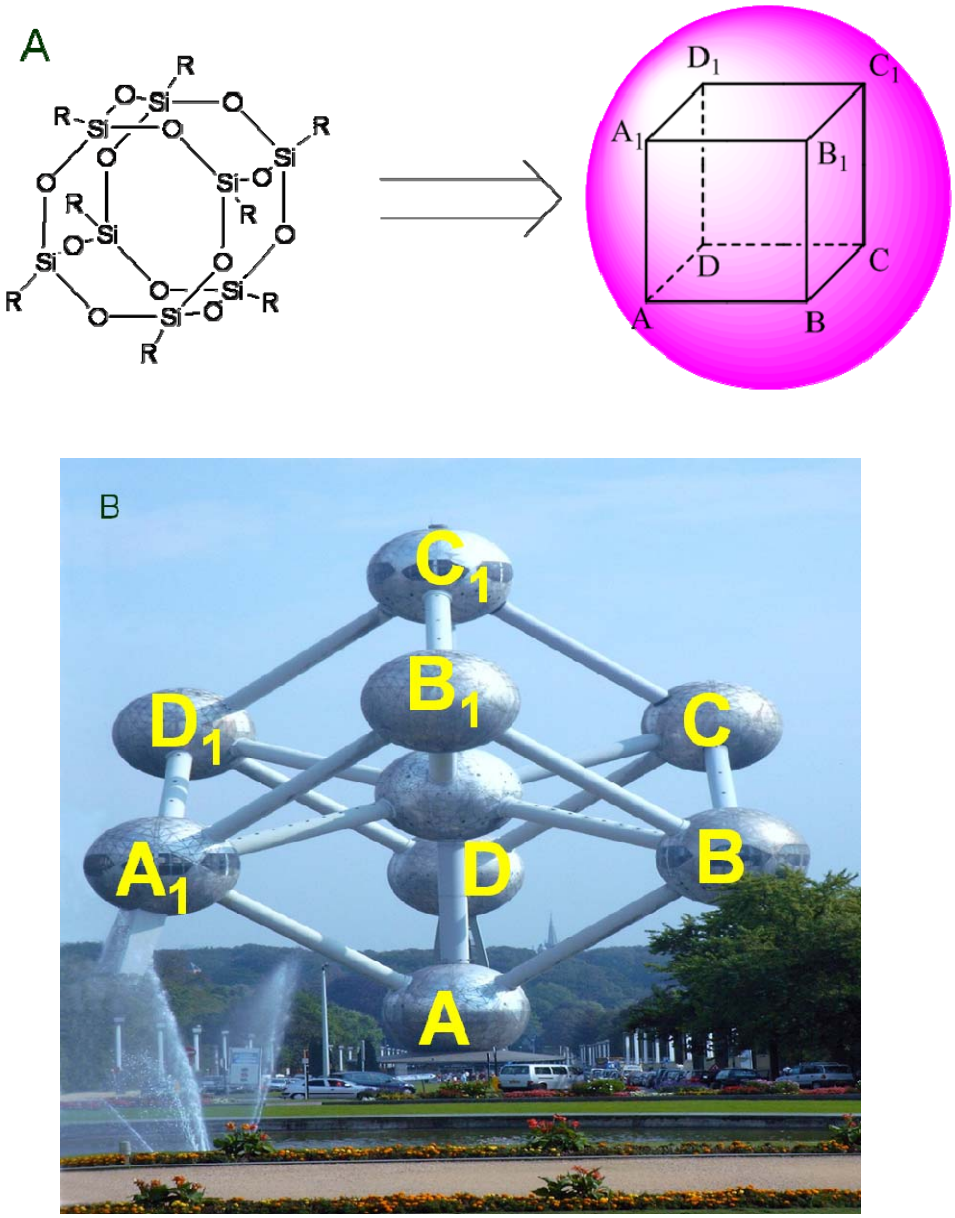

Figure 3.9 (A) The T_8 POSS cage was treated as an ideal cube with the substituents evenly distributed at the vertices of the cage. In this model, *Si* atoms are located at the eight corners of the cube while omitted *O* atoms are in the middle of the 12 edges. (**B**) The Atomium for Brussels World's Fair.[73] The labeling of the cube in (**A**) and Atomium in (**B**) are consistent with balancing the cube on vertex A for a vertex-on conformation.

The subsequent discussion of T_8 POSS cages are inspired by the models in Figure 3.9. In order to simplify this calculation, we can consider a T_8 POSS cage as an ideal cube *ABCD-$A_1B_1C_1D_1$* where the substituents R are distributed evenly at each vertex of the cube and fill out the pink sphere (in Figure 3.9A). In this model, silicon atoms are located on the eight corners while omitted oxygen atoms are in the middle of the 12 edges. Therefore, the sizes (limiting area) of the POSS derivatives are effectively spherical areas determined by the largest cross-sectional areas.

If the molecule is tilted on one corner, *A*, as proposed for TiBP,[65e] a vertex-on conformation would be observed that would look like the labeled "Atomium" built for the World's Fair in Brussels (Figure 3.9B). As shown in Figure 3.9B, its largest cross-sectional area would be the circumcircle of the triangle *A_1BD* or *B_1CD_1*. If we assume *AA_1*, the side length of the cube *ABCD-$A_1B_1C_1D_1$*, is *a*, $A_1B = BD = A_1D = \sqrt{2}a$ indicating an equilateral triangle *A_1BD* as shown in Figure 3.10. Their perpendicular bisectors *A_1E*, *BG*, and *DF* pass through vertices and intersect at *O_1*, the center of the circle. As the areas of triangles *AO_1B*, *A_1O_1D*, and *BO_1D* are equal, the area of triangle *BO_1D* is equivalent to 1/3 of the area of triangle *A_1BD*. Hence,

$$\frac{1}{2}(BD \times O_1E_1) = \frac{1}{3} \times \frac{1}{2}(BD \times A_1E_1) \tag{3.1}$$

$$3\ O_1E_1 = A_1E_1 = A_1O_1 + O_1E_1 \tag{3.2}$$

$$r_1 = A_1O_1 = 2\ O_1E_1 = \frac{2}{3}A_1E_1 = \frac{2}{3}\left(\frac{\sqrt{3}}{2}BD\right) = \frac{2}{3}\left(\frac{\sqrt{3}}{2} \times \sqrt{2}a\right) = \frac{\sqrt{6}}{3}a \tag{3.3}$$

Therefore, the area of circumcircle O_1 (S_1):

$$S_1 = \pi {r_1}^2 = \pi\left(\frac{\sqrt{6}}{3}a\right)^2 = \frac{2}{3}\pi a^2 \tag{3.4}$$

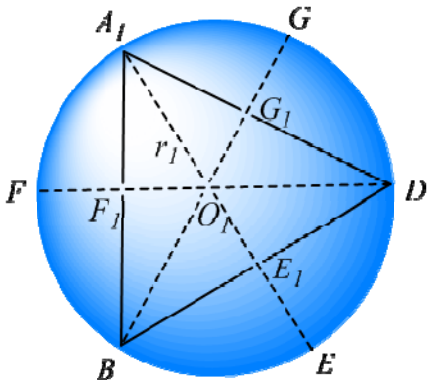

Figure 3.10 Circumcircle O_1 of equilateral triagle A_1BD. A_1E, BG, and DF are perpendicular bisectors of BD, A_1D, and A_1B and intersect at E_1, G_1, and F_1, respectively. r_1 represents the radius of the circumcircle O_1.

On the other hand, if the POSS cage is packed on one of its faces, the biggest cross-sectional area is the circumcircle of the square $ABCD$ or $A_1B_1C_1D_1$ and turns out to be the face-on conformation. As shown in Figure 3.11, if we still consider the side length of the tube $ABCD$-$A_1B_1C_1D_1$ as a, the effective radius of the circumcircle, and the area of circumcircle O_2 (S_2) is:

$$r_2 = DO_2 = \frac{\sqrt{2}}{2} AB = \frac{\sqrt{2}}{2} a \tag{3.5}$$

$$S_2 = \pi r_2^2 = \pi \left(\frac{\sqrt{2}}{2} a\right)^2 = \frac{1}{2} \pi a^2 \tag{3.6}$$

Therefore, the ratio of largest spherical areas between a vertex-on conformation (S_1) and a face-on conformation (S_2) is 4:3. Since the limiting area of TiBP is $A_0 \sim 177$ Å^2·molecule^{-1}, the limiting area of a POSS molecule on its face should be ~ 130 Å^2·molecule^{-1}. This value is in

accord with the observed limiting area for POSS-OH and POSS-triacid. On the basis of these experiments, I would propose that POSS cages with longer tethering chains or fewer hydrophilic end groups tend to lie on one of the six faces of the molecule at the A/W interface.

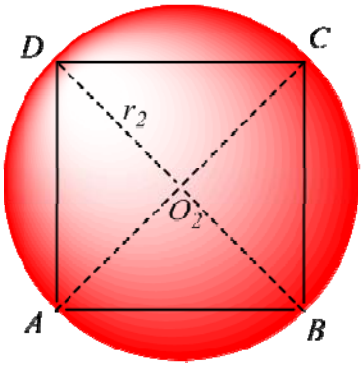

Figure 3.11 Circumcircle O_2 of the square *ABCD*. Two diagonals *AC* and *BD* intersect at O_2, the center of the circumcircle. r_2 represents the radius of circumcircle O_2.

3.8 Other POSS Molecules that Exhibit Face-on Conformations

In order to test this hypothesis, experiments on other compounds were performed. POSS materials with seven isobutyl substituents, and an eighth hydrophilic substituent like an aminopropyl group (POSS-NH_2) or propylmethyacrylate (POSS-MA) were considered (Figure 3.12).

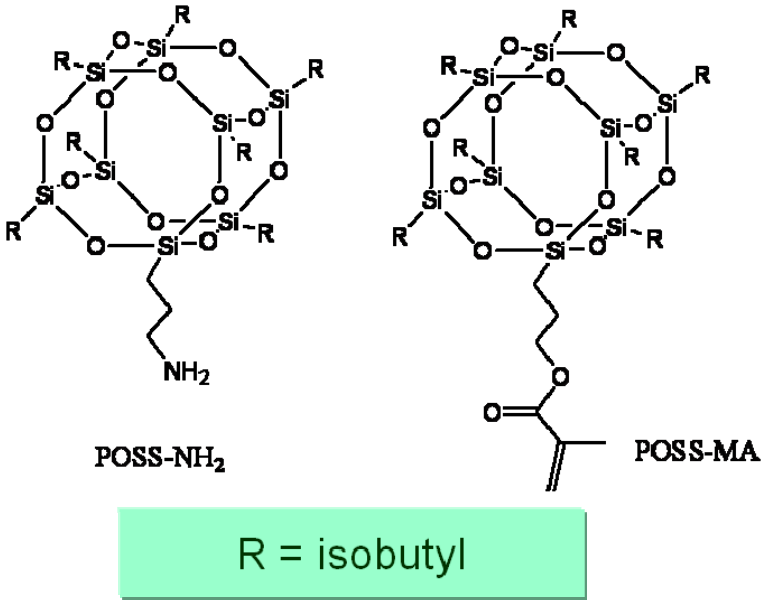

Figure 3.12 Chemical structures of POSS-NH_2 and POSS-MA.

$\prod$-*A* isotherms for POSS-NH_2 and POSS-MA are provided in Figure 3.13. As seen in Figure 3.13, $A_{lift\text{-}off} \approx A_0$ = 130 Å^2·molecule^{-1} for POSS-NH_2 and $A_{lift\text{-}off} \approx A_0$ = 125 Å^2·molecule^{-1} for POSS-MA. These values are consistent with the results observed for POSS-OH and POSS-triacid. Furthermore, the shapes of the POSS-NH_2 and POSS-MA isotherms are similar to POSS-OH. All three isotherms exhibit plateaus after collapse of the films. For POSS-MA, collapse occurs at A_c = 110 Å^2·molecule^{-1} and $\prod_c$ = 3 mN·m^{-1} with a plateau from 75 Å^2•molecule^{-1} < *A* < 110 Å^2•molecule^{-1}, whereas collapse for POSS-NH_2 starts at A_c = 120 Å^2·molecule^{-1} and $\prod_c$ = 17 mN·m^{-1} with a plateau from 80 Å^2•molecule^{-1} < *A* < 120 Å^2•molecule^{-1}. The difference in collapse pressures between the $\prod_{c,\ POSS\text{-}MA} < \prod_{c,\ POSS\text{-}OH} < \prod_{c,\ POSS\text{-}NH2}$ reflects stronger interactions between the hydrophilic moiety and the subphase. As seen in Figure 3.13, $\prod_c$ for POSS-triacid is in excess of 35 mN·m^{-1}. Furthermore, POSS-NH_2 and POSS-MA exhibit

increases in ∏ at small *A* that are similar to POSS-OH. On the basis of these observations, it appears that POSS-MA and POSS-NH_2 also pack in face-on conformations.

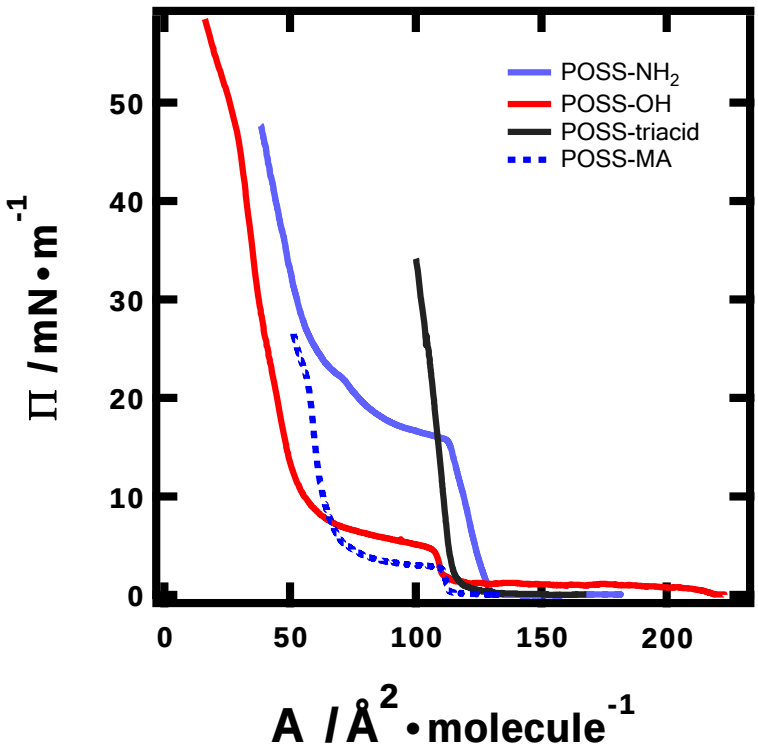

Figure 3.13 ∏-*A* isotherms for isobutyl substituted POSS derivatives: POSS-NH_2, POSS-OH, POSS-triacid, and POSS-MA on the A/W interface (T = 22.5 ^{o}C).

3.9 Possible Conformations for POSS-triester in Langmuir Films at the A/W Interface

In order to understand why the film of POSS-triester forms a LE monolayer, it is useful to consider the Π-*A* isotherm for poly(t-butyl acrylate) (PtBA). Figure 3.14A shows a Π-*A* isotherm for PtBA where A is expressed as a function of the area per repeating unit (monomer for short). As seen in Figure 3.14A, Π for the PtBA film initially shows a slow rise in the region $35 < A < 55$ Å^2·molecule^{-1} = $A_{lift\text{-}off,\ PtBA}$. Further compression of the film causes Π to rise rapidly for $A <$ 35 Å^2·molecule^{-1} before the film collapses at $A_c \sim 21$ Å^2·molecule^{-1} and $\Pi_c \sim 23$ mN·m^{-1}. The rapid rise in Π for $A < 35$ Å^2·molecule^{-1} is consistent with the formation of a condensed (LC) film. Extrapolation of the Π-*A* isotherm for the LC monolayer back to Π = 0 yields $A_0 \approx 30$ Å^2·molecule^{-1}. As seen in Figure 3.14B if one neglects the short linker, POSS-triester is essentially POSS-OH plus three PtBA repeating units. Interestingly, $A_{0,\ POSS\text{-}OH} + 3A_{0,PtBA}$ yields 215 Å^2·molecule^{-1} ($\approx A_{lift\text{-}off,\ POSS\text{-}triester}$). As such, we speculate that POSS-triester starts with the POSS-cage and three *tert*-butyl esters adsorbed to the plane of the interface (Figure 3.15A). Throughout the monolayer regime, the POSS cage is likely riding on top of the *tert*-butyl esters (Figure 3.15B). Recalling that TiBP and POSS-triester Π-*A* isotherms essentially coincided throughout the monolayer regime (Figure 3.6), a somewhat more speculative conclusion is that the POSS cage tilts during the transformation from a cage on the A/W interface to a cage on the *tert*-butyl esters as depicted in Figure 3.15B. However, there is a difference in A_c between POSS-triester and TiBP. TiBP collapsed at $A_c = 140$ Å^2·molecule^{-1}, whereas POSS-triester collapsed at a smaller $A_c = 125$ Å^2·molecule^{-1}. This value is consistent with a face-on conformation for POSS-triester at collapse (Figure 3.15C).

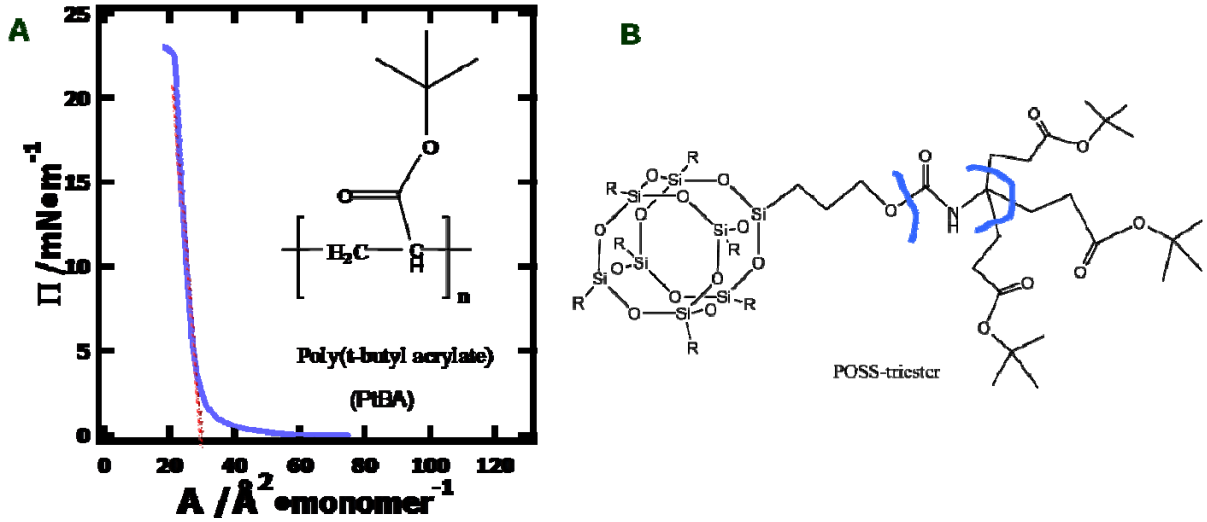

Figure 3.14 (**A**) Π-*A* isotherm for PtBA on water at T= 22.5 °C. The red dashed line indicates A_0 for PtBA. (**B**) Structure of POSS-triester highlighting the POSS-OH piece and the three PtBA "repeating units".

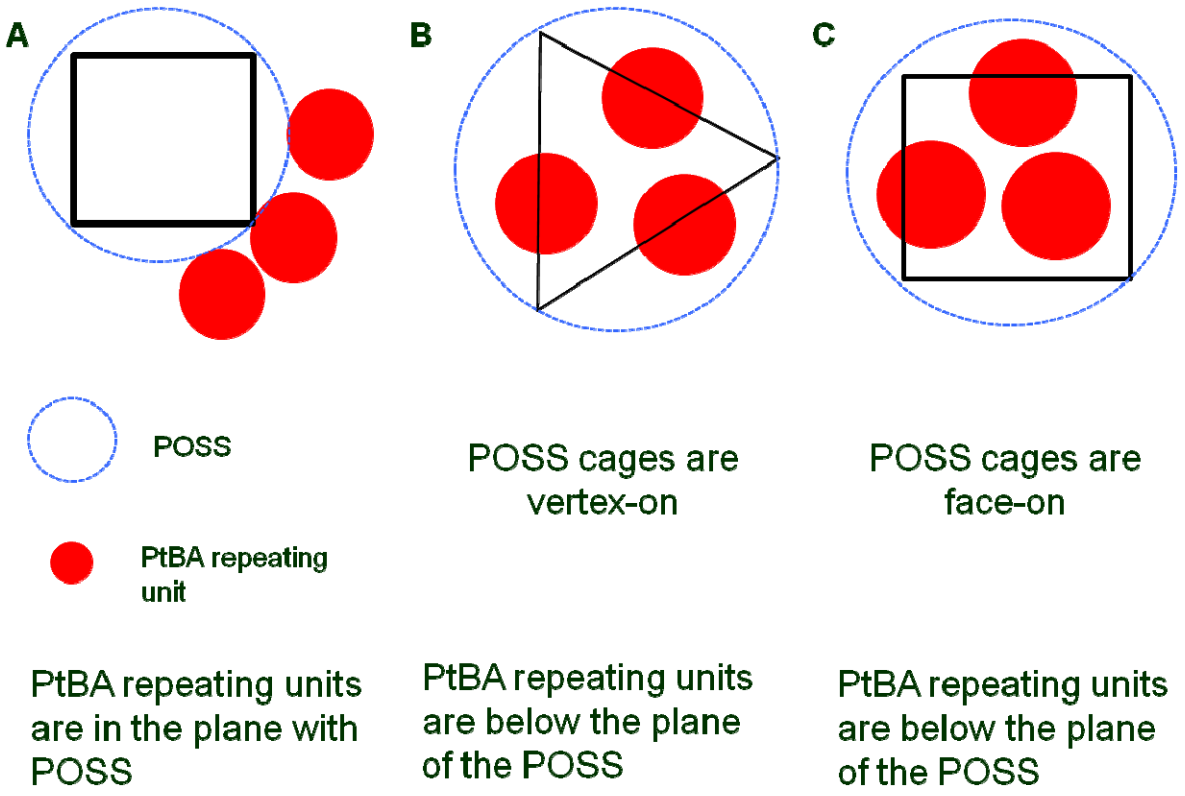

Figure 3.15 Schematic depictions of POSS-triester (top view) in Langmuir films at various A: (**A**) $A = A_{lift\text{-}off}$, (**B**) $A_c < A < A_{lift\text{-}off}$, and (**C**) $A = A_c$.

3.10 Summary

Two new POSS derivatives, POSS-triester and POSS-triacid were synthesized and completely characterized. A third derivative POSS-OH was purified. Π-A isotherm studies of these molecules were consistent with face-on conformations at the A/W interface for the POSS cages prior to collapse in contrast to trisilanol-POSS derivatives which appear to pack in a vertex-on

conformation. Subsequently, POSS-NH_2 and POSS-MA also had limiting areas consistent with face-on conformations. These studies provide new insights into design and interfacial properties of silicon based surfactants and surface modifying agents.

Chapter 4

Suggestions for Future Work

4.1 Π-*A* Isotherms of POSS Amphiphiles

Figure 4.1 contains surface pressure-area per molecule (Π-*A*) isotherms for POSS-OH and POSS-triester from Chapter 3 (Figure 3.6).

As one may notice in Figure 4.1, there is a "window" with respect to packing at the A/W interface between the POSS-OH and POSS-triester. It is my desire to design, synthesize, and characterize POSS molecules to fill this "window". I suggest to start with a POSS-OH based diester (**6**) (Scheme 4.1) with the help of a diester-isocyanate (provided by Brad Maisuria from Dr. Richard D. Gandour's research group) to create a molecule that will be less hydrophilic and have a smaller cross-sectional area at $A_{lift\text{-}off}$ (area where Π derivates from zero). It will be interesting to examine the packing of the **6** during compression. Either vertex-on or face-on orientations, or even a conformation that lies somewhere in-between will be helpful for understanding how POSS cages pack at the A/W interface. I suggest to convert **6** into the corresponding POSS-OH based diacid (**7**). The rigidity of the monolayer films may differ from POSS-triester and POSS-triacid in Chapter 3 because of weaker intermolecular interactions. In preliminary work, **6** has been synthesized and characterized by ^{1}H NMR (Figure 4.2).

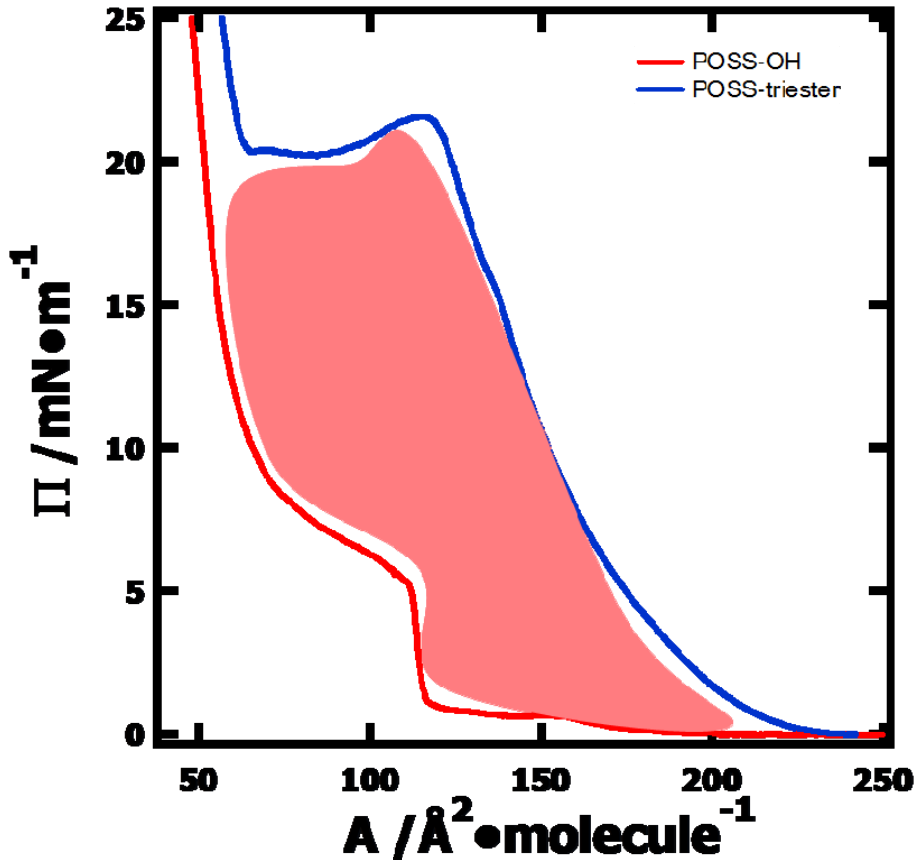

Figure 4.1 Π-*A* isotherm comparisons of POSS-OH and POSS-triester at the A/W interface at 22.5 °C. The shaded peach region represents a region of interest for controlling POSS packing through the synthesis of new POSS amphiphiles.

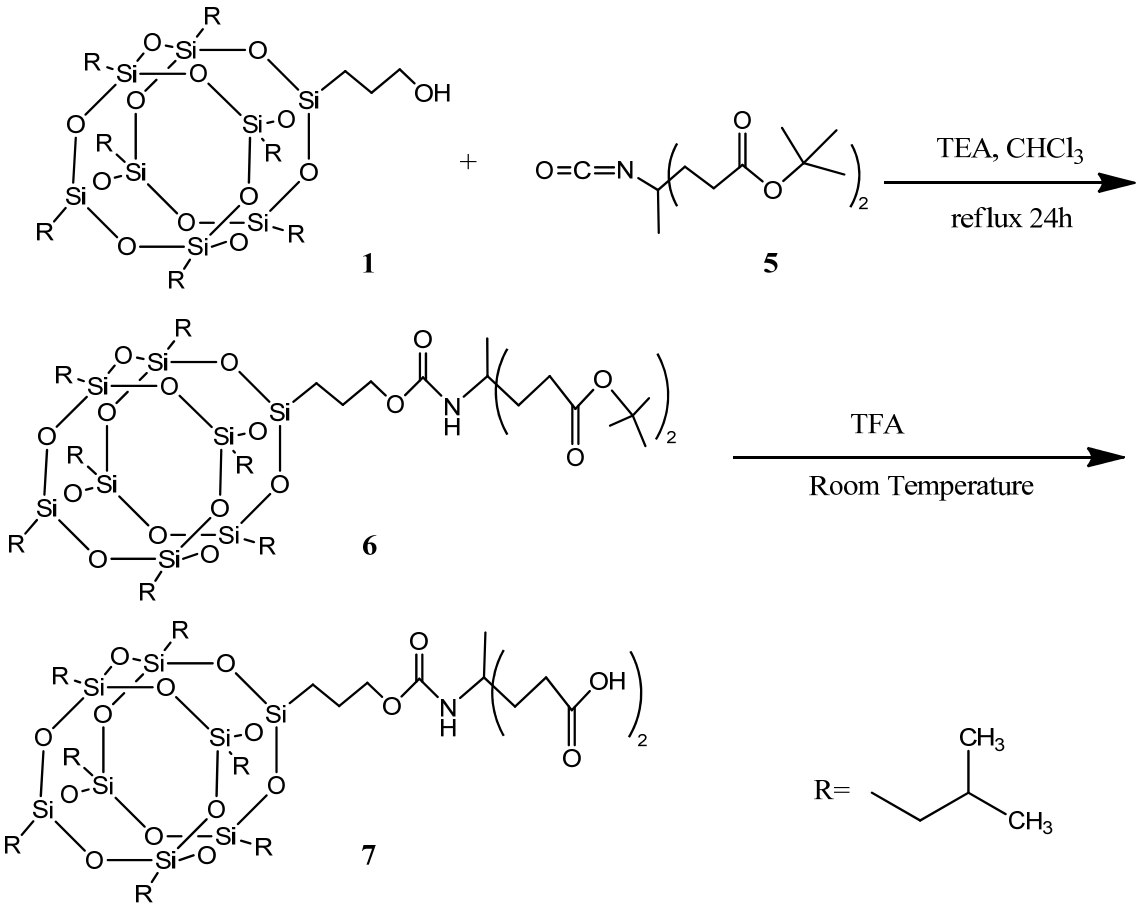

Scheme 4.1 Synthesis of POSS-OH based diester (**6**) and diacid (**7**).

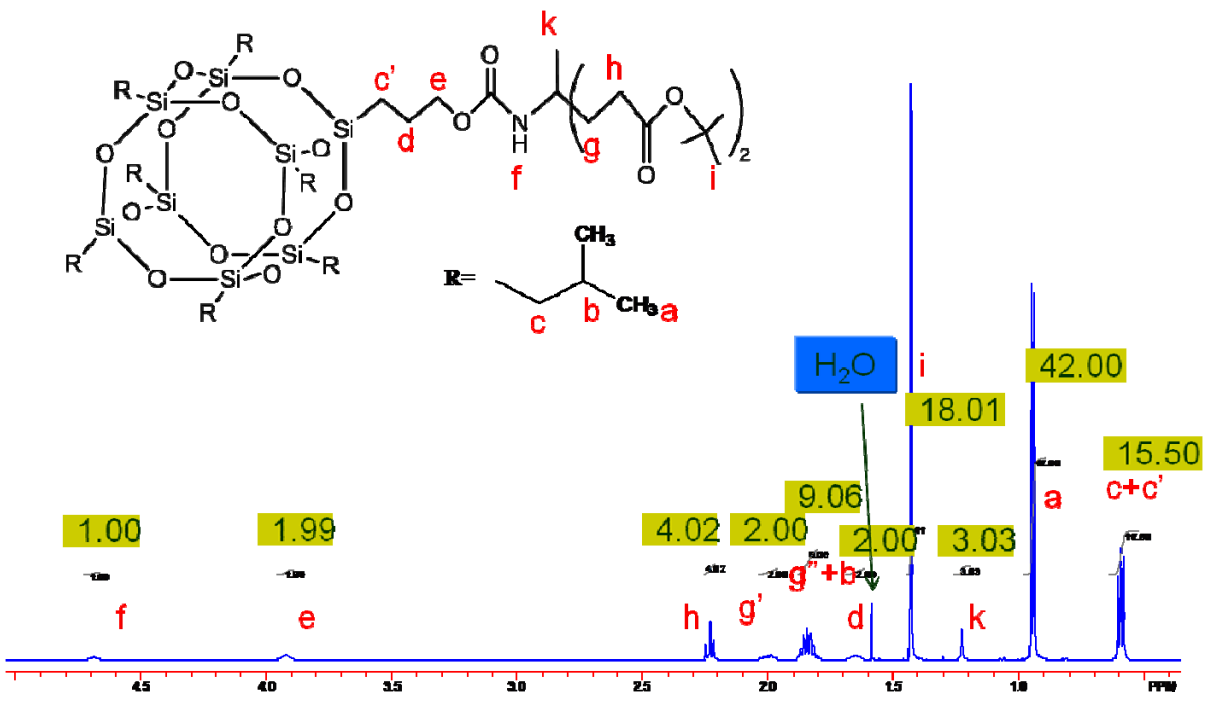

Figure 4.2 ^{1}H NMR of POSS-OH based diester (**6**).

4.2 POSS Amphiphiles Based on POSS-NH_2

Figure 4.3 is a comparison of Π-*A* isotherms for POSS-NH_2 and POSS-OH from Chapter 3. Besides similar limiting areas (A_0) that are consistent with face-on conformations, similar collapse areas (A_c) ≈ 110 Å^2·molecule^{-1} indicate that they both aggregate to form multilayers at the same molecular area. However, the collapse pressure of POSS-OH is much smaller (~ 1/4 that of POSS-NH_2), indicating that the interactions between POSS-NH_2 and water are much stronger than those between POSS-OH and water. Therefore, POSS-NH_2 derived esters and acids may show monolayer properties that differ from POSS-OH derived esters and acids. Therefore I suggest using POSS-NH_2 to make POSS-NH_2 based triesters and triacids following an approach

that is analogous to the one using POSS-OH in Chapter 3 (Scheme 4.2). One key advantage is that the price of POSS-NH_2 is lower. In preliminary work, **10** has been synthesized and characterized by ^{1}H NMR (Figure 4.4).

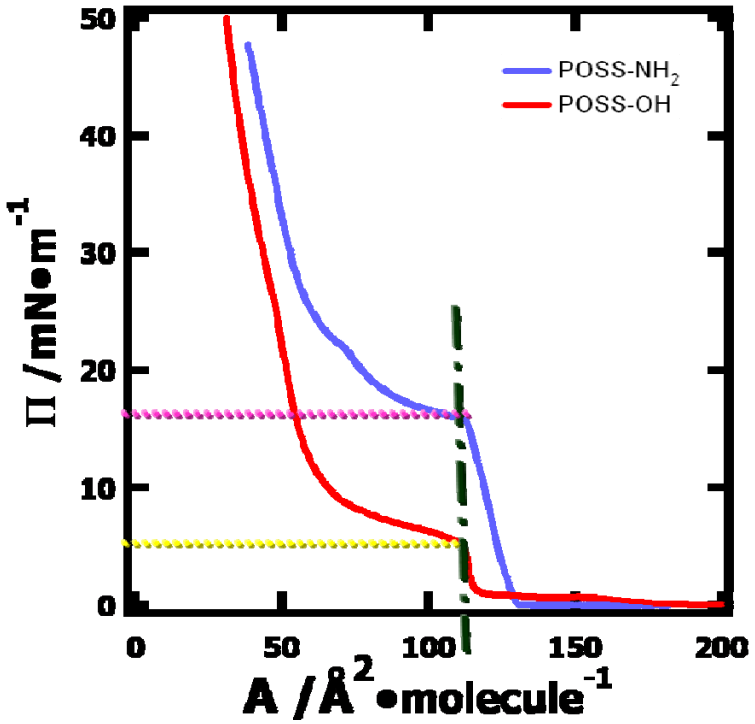

Figure 4.3 Π-*A* isotherm comparisons of POSS-OH and POSS-NH_2 at the A/W interface at 22.5 °C.

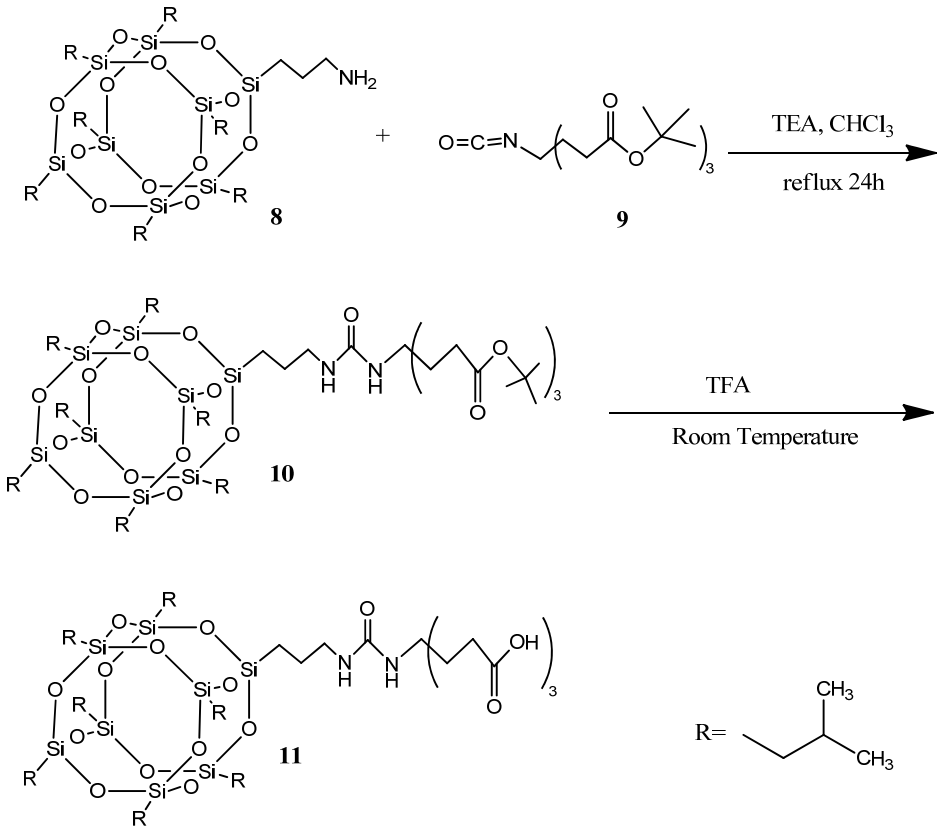

Scheme 4.2 Synthesis of POSS-NH_2 based triester (**10**) and triacid (**11**).

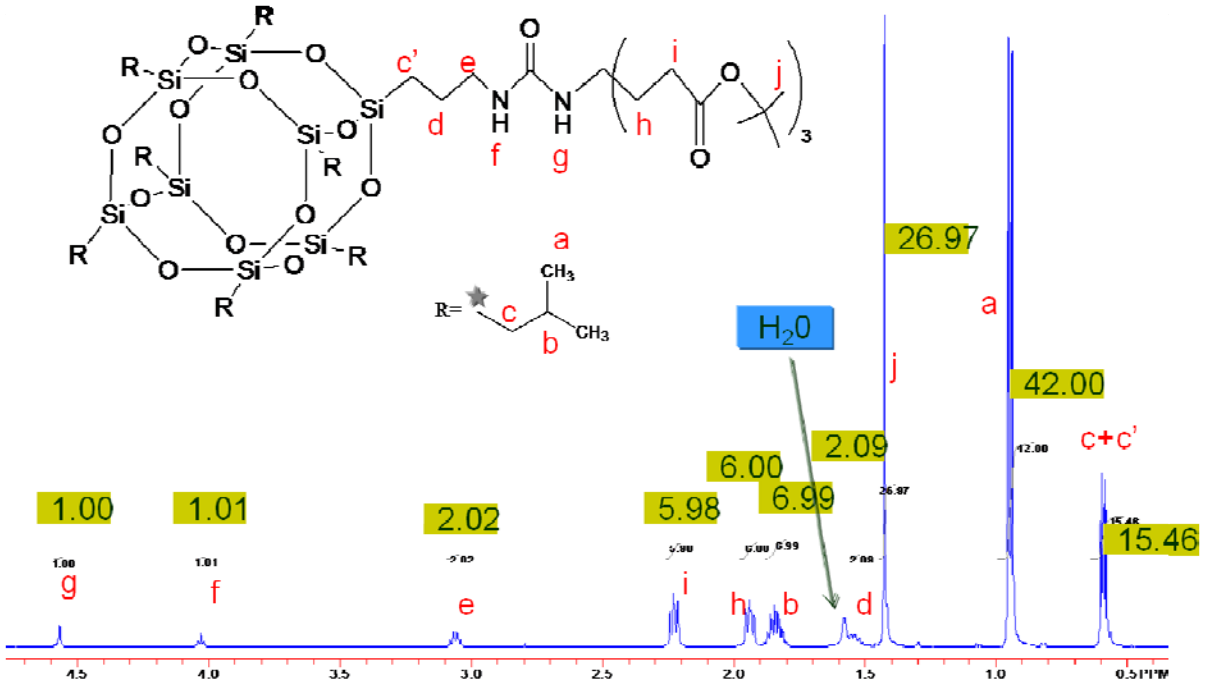

Figure 4.4 ^{1}H NMR of POSS-NH_2 based triester.

4.3 Other POSS Esters

Another way to explore the "window" is to synthesize different esters by coupling different alcohols to diacids and triacids based on POSS-OH or POSS-NH_2. It would also be attractive to study and compare their surface properties via isotherms and BAM with respect to molecular orientation and rigidity. For example, POSS-triester with t-butyl groups should be larger than POSS-OH based trimethylester (POSS-TME). On the other hand, POSS-TME could be more rigid than POSS-triester owing to a less bulky and more hydrophilic head group and

consequently stronger intermolecular interactions with water. However, no matter which esters are used, I ultimately expect the POSS cages to pack in the face-on conformation at high Π.

4.4 POSS-derivatives with Different Substituents

To this point, the POSS derivatives have had the same R substituent (isobutyl). It is also possible to vary R through the amine-based linking chemistry. I plan to expand the library of T_8 POSS based triesters and triacids by creating amine functionalized branches from trisilanol POSS derivatives with different substituents.[74] An approach to synthesize phenyl substituted POSS-NH_2 is shown in Scheme 4.3.

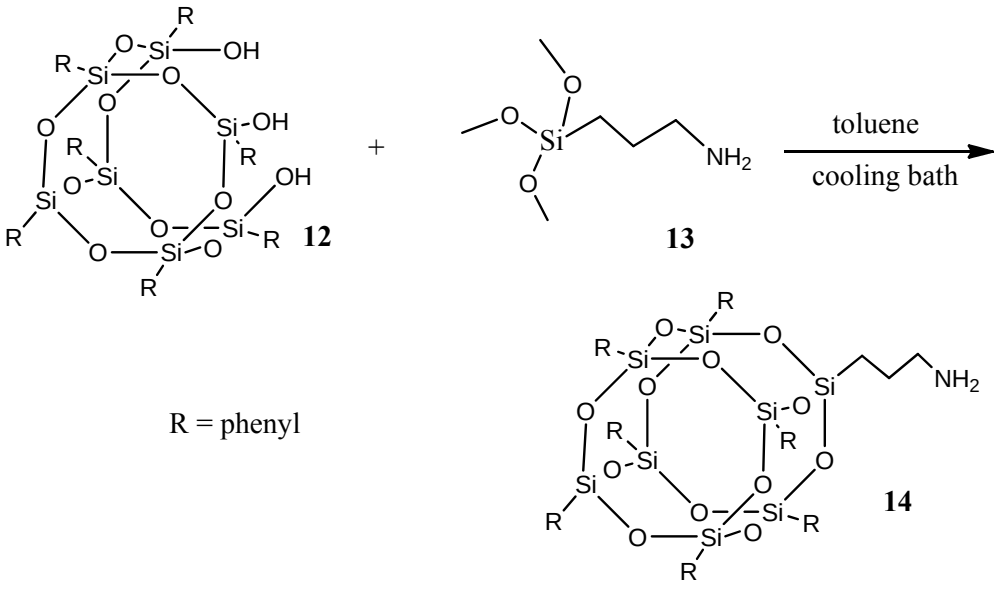

Scheme 4.3 Synthesis of phenyl substituted POSS-NH_2 from a trisilanol-POSS.[75]

4.5 POSS-based Nanofillers in Polydimethylsiloxane at the A/W Interface

Ultimately, I suggest using these new POSS derivatives to examine how they behave as nanofillers in Langmuir films. Polydimethylsiloxane **(**PDMS) is a material known to form stable flexible monolayers and multilayers at the A/W interface.[76] Blends of PDMS and trisilanol-POSS derivatives at the A/W interface have examined aggregate formation[77] and rheological properties.[34, 78] Since closed-cage POSS are normally non-amphiphilic and tend to form rigid multilayer aggregates at the A/W interface, octaalkyl-POSS/PDMS blends show filler reinforcement with PDMS induced dispersion of the closed-cage POSS.[67a] The POSS-based triester and triacid derivatives I have made are also closed-cage; however, the hydrophilic arm makes them amphiphilic. As such, I hypothesize these materials can significantly enhance the dilational modulus of PDMS films at the A/W interface.

Bibliography

1. Hans-Jurgen Butt, K. G., Michael Kappl, Physics and chemistry of Interfaces. **2003**.
2. (a) Smirnova, Y. G.; Marrink, S.-J.; Lipowsky, R.; Knecht, V., Solvent-Exposed Tails as Prestalk Transition States for Membrane Fusion at Low Hydration. *J. Am. Chem. Soc.* **2010,** *132* (19), 6710-6718; (b) Schneggenburger, P. E.; Muellar, S.; Worbs, B.; Steinem, C.; Diederichsen, U., Molecular Recognition at the Membrane-Water Interface: Controlling Integral Peptide Helices by Off-Membrane Nucleobase Pairing. *J. Am. Chem. Soc.* **2010,** *132* (23), 8020-8028; (c) Nagata, Y.; Mukamel, S., Vibrational Sum-Frequency Generation Spectroscopy at the Water/Lipid Interface: Molecular Dynamics Simulation Study. *J. Am. Chem. Soc.* **2010,** *132* (18), 6434-6442; (d) Jurak, M.; Chibowski, E., Influence of (phospho)lipases on properties of mica supported phospholipid layers. *Applied Surface Science* **2010,** *256* (21), 6304-6312.
3. (a) Prakash, B. S. J., Surface thermodynamics of clays. *Interface Science and Technology* **2004,** *1* (Clay Surfaces), 90-117; (b) Kaneko, M. L. Q. A.; Yoshida, I. V. P., Effect of natural and organically modified montmorillonite clays on the properties of polydimethylsiloxane rubber. *J. Appl. Polym. Sci.* **2008,** *108* (4), 2587-2596; (c) Deka, M.; Kumar, A., Enhanced electrical and electrochemical properties of PMMA-clay nanocomposite gel polymer electrolytes. *Electrochimica Acta* **2010,** *55* (5), 1836-1842.
4. (a) Stine, C. M.; Patton, S., Preparation of milk fat. II. A new method of manufacturing butter oil. *Journal of Dairy Science* **1952,** *35*, 655-60; (b) Segall, K. I.; Goff, H. D., Secondary adsorption of milk proteins from the continuous phase to the oil-water interface in dairy emulsions. *International Dairy Journal* **2002,** *12* (11), 889-897; (c) Pelan, B. M. C.; Watts, K. M.; Campbell, I. J.; Lips, A., The stability of aerated milk protein emulsions in the presence of small molecule surfactants. *Journal of Dairy Science* **1997,** *80* (10), 2631-2638; (d) Jebson, R. S., Butter and allied products. *Fats Food Prod.* **1994**, 69-109.
5. (a) Molina, R.; Esquena, J.; Erra, P., Interfacial processes in textile materials: relevance to adhesion. *Journal of Adhesion Science and Technology* **2010,** *24* (1), 7-33; (b) Foose, L. L. Proteolysis of immobilized proteins at the solid/aqueous interface: Implications for detergency. 2008.
6. (a) Wasyluk, J.; Perova, T. S.; Kukushkin, S. A.; Osipov, A. V.; Feoktistov, N. A.; Grudinkin, S. A., Raman investigation of different polytypes in SiC thin films grown by solid-gas phase epitaxy on Si (111) and 6H-SiC substrates. *Materials Science Forum* **2010,** *645-648* (Pt. 1, Silicon Carbide and Related Materials 2009), 359-362; (b) Sumigawa, T.; Shishido, T.; Murakami, T.; Kitamura, T., Interface crack initiation due to nano-scale stress concentration. *Materials Science & Engineering, A: Structural Materials: Properties, Microstructure and Processing* **2010,** *527* (18-19), 4796-4803; (c) Jahromi, S. S.; Masoudi, S. F., Detection of nano scale thin films with polarized neutron reflectometry at the presence of smooth and rough interfaces. *Appl. Phys. A Mater. Sci. Process.* **2010,** *99* (1), 255-263.
7. (a) Wang, P.; Schaefer, D. W., Hygrothermal aging of silane-laced epoxy coatings. *Journal of Adhesion Science and Technology* **2010,** *24* (4), 699-708; (b) Singh, A.; Bakshi, S. R.; Agarwal, A.; Harimkar, S. P., Microstructure and tribological behavior of spark plasma sintered iron-based amorphous coatings. *Materials Science & Engineering, A: Structural Materials: Properties, Microstructure and Processing* **2010,** *527* (18-19), 5000-5007; (c) Huang, Y.; Zeng, X., Investigation on cracking behavior of Ni-based coating by laser-induction hybrid cladding. *Applied Surface Science* **2010,** *256* (20), 5985-5992; (d) Corwin, A. D.; de Boer, M. P., Frictional aging, de-aging, and re-aging in a monolayer-coated micromachined interface. *Physical Review B: Condensed Matter and Materials Physics* **2010,** *81* (17), 174109/1-174109/11.

8. (a) Zhang, J.; Li, R.; Yu, Q., Effect of plasma interface treatment and cathodic electrophoretic coating on Mg alloys. *Materials Science Forum* **2009,** *610-613* (Pt. 2, Materials Research: Eco/Environmental Materials, Energy Materials, Magnesium, Aerospace Materials and Biomaterials for Medical Application), 984-990; (b) Liu, J.; Chaudhury, M. K.; Berry, D. H.; Seebergh, J. E.; Osborne, J. H.; Blohowiak, K. Y., Effect of processing conditions on adhesion performance of a sol-gel reinforced epoxy/aluminum interface. *Journal of Adhesion Science and Technology* **2008,** *22* (10-11), 1159-1180; (c) Gruchow, F.; Machill, S.; Thiele, S.; Herm, C.; Salzer, R., Imaging FTIR spectroscopic investigations of wood: paint interface of aged polychrome art objects. *e-Preservation Science* **2009,** *6*, 145-150.
9. Panayiotou, C., Interfacial tension and interfacial profiles of fluids and their mixtures. *Langmuir* **2002,** *18* (23), 8841-8853.
10. (a) Pielichowski, K.; Njuguna, J.; Janowski, B.; Pielichowski, J., Polyhedral oligomeric silsesquioxanes (POSS)-containing nanohybrid polymers. *Adv. Polym. Sci.* **2006,** *201* (Supramolecular Polymers, Polymeric Betains, Oligomers), 225-296; (b) Gonzalez, R. I.; Phillips, S. H.; Hoflund, G. B., In situ oxygen-atom erosion study of polyhedral oligomeric silsesquioxane-siloxane copolymer. *Journal of Spacecraft and Rockets* **2000,** *37* (4), 463-467; (c) Hacker, N. P., *MRS Bulletin* **1997,** *22*, 33; (d) Laine, R. M.; Zhang, C.; Sellinger, A.; Viculis, L., Polyfunctional cubic silsesquioxanes as building blocks for organic/inorganic hybrids. *Appl. Organomet. Chem.* **1998,** *12* (10/11), 715-723; (e) Duchateau, R.; Abbenhuis, H. C. L.; van Santen, R. A.; Meetsma, A.; Thiele, S. K. H.; van Tol, M. F. H., Ethylene Polymerization with Dimeric Zirconium and Hafnium Silsesquioxane Complexes. *Organometallics* **1998,** *17* (26), 5663-5673; (f) Laine, R. M., Nanobuilding blocks based on the [OSiO1.5]x (x = 6, 8, 10) octasilsesquioxanes. *J. Mater. Chem.* **2005,** *15* (35-36), 3725-3744; (g) Provatas, A.; Matisons, J. G., Silsesquioxanes: synthesis and applications. *Trends Polym. Sci. (Cambridge, U. K.)* **1997,** *5* (10), 327-332; (h) Baney, R. H.; Itoh, M.; Sakakibara, A.; Suzuki, T., Silsesquioxanes. *Chem. Rev. (Washington, D. C.)* **1995,** *95* (5), 1409-30; (i) Voronkov, M. G.; Lavrent'yev, V. I., Polyhedral oligosilsesquioxanes and their homo derivatives. *Top. Curr. Chem.* **1982,** *102*, 199-236; (j) Iacono, S. T.; Budy, S. M.; Mabry, J. M.; Smith, D. W., Jr., Synthesis, Characterization, and Surface Morphology of Pendant Polyhedral Oligomeric Silsesquioxane Perfluorocyclobutyl Aryl Ether Copolymers. *Macromolecules (Washington, DC, U. S.)* **2007,** *40* (26), 9517-9522.
11. Harrison, P. G., Silicate cages: precursors to new materials. *J. Organomet. Chem.* **1997,** *542* (2), 141-183.
12. (a) Feher, F. J.; Budzichowski, T. A., Silasesquioxanes as ligands in inorganic and organometallic chemistry. *Polyhedron* **1995,** *14* (22), 3239-3253; (b) Carniato, F.; Boccaleri, E.; Marchese, L., A versatile route to bifunctionalized silsesquioxane (POSS): synthesis and characterisation of Ti-containing aminopropylisobutyl-POSS. *Dalton Trans* **2008,** (1), 36-39; (c) Mantz, R. A.; Jones, P. F.; Chaffee, K. P.; Lichtenhan, J. D.; Gilman, J. W.; Ismail, I. M. K.; Burmeister, M. J., Thermolysis of Polyhedral Oligomeric Silsesquioxane (POSS) Macromers and POSS-Siloxane Copolymers. *Chem. Mater.* **1996,** *8* (6), 1250-1259.
13. (a) Sprung, M. M.; Guenther, F. O., The partial hydrolysis of methyltriethoxysilane. *J. Am. Chem. Soc.* **1955,** *77*, 3990-3996; (b) Barry, A. J.; Daudt, W. H.; Domicone, J. J.; Gilkey, J. W., Crystalline organosilsesquioxanes. *J. Am. Chem. Soc.* **1955,** *77*, 4248-4252; (c) Vogt, L. H., Jr.; Brown, J. F., Jr., Crystalline methylsilsesquioxanes. *Inorg. Chem. (Washington, DC, U. S.)* **1963,** *2*, 189-192.
14. Feher, F. J.; Budzichowski, T. A.; Blanski, R. L.; Weller, K. J.; Ziller, J. W., Facile syntheses of new incompletely condensed polyhedral oligosilsesquioxanes: [(c-C5H9)7Si7O9(OH)3], [(c-C7H13)7Si7O9(OH)3], and [(c-C7H13)6Si6O7(OH)4]. *Organometallics* **1991,** *10* (7), 2526-2528.
15. (a) Feher, F. J.; Soulivong, D.; Lewis, G. T., Facile Framework Cleavage Reactions of a Completely Condensed Silsesquioxane Framework. *J. Am. Chem. Soc.* **1997,** *119* (46), 11323-11324; (b) Feher, F. J.; Nguyen, F.; Soulivong, D.; Ziller, J. W., A new route to incompletely condensed silsesquioxanes: acid-mediated cleavage and rearrangement of (c-C6H11)6Si6O9 to C2-[(c-C6H11)6Si6O8X2]. *Chem. Commun. (Cambridge)* **1999,** (17), 1705-1706; (c) Feher, F. J.; Soulivong, D.; Nguyen, F., Practical methods for

synthesizing four incompletely condensed silsesquioxanes from a single R8Si8O12 framework. *Chem. Commun. (Cambridge)* **1998,** (12), 1279-1280.
16. Schwab, J. J.; Lichtenhan, J. D., Polyhedral oligomeric silsesquioxane (POSS)-based polymers. *Appl. Organomet. Chem.* **1998,** *12* (10/11), 707-713.
17. Lee, Y.-J.; Huang, J.-M.; Kuo, S.-W.; Chang, F.-C., Low-dielectric, nanoporous polyimide films prepared from PEO-POSS nanoparticles. *Polymer* **2005,** *46* (23), 10056-10065.
18. Yen, Y.-C.; Kuo, S.-W.; Huang, C.-F.; Chen, J.-K.; Chang, F.-C., Miscibility and Hydrogen-Bonding Behavior in Organic/Inorganic Polymer Hybrids Containing Octaphenol Polyhedral Oligomeric Silsesquioxane. *J. Phys. Chem. B* **2008,** *112* (35), 10821-10829.
19. (a) Iacona, S. T.; Budy, S. M.; Smith, R. C.; Neilson, A. R.; Ballato, J.; Smith, D. W., Step-Growth Polyaddition and Polycondensation Reactions of Aromatic Trifluorovinyl Ethers. *Abstracts, 42nd Western Regional Meeting of the American Chemical Society, Las Vegas, NV, United States, September 23-27* **2008**, WRM-176; (b) Pyun, J.; Miller, P. J.; Matyjaszewski, K.; Kickelbick, G.; Schwab, J.; Lichtenhan, J. D., Synthesis of organic/inorganic hybrid materials from polysiloxane precursors using atom-transfer radical polymerization. *Book of Abstracts, 218th ACS National Meeting, New Orleans, Aug. 22-26* **1999**, POLY-513; (c) Kolel-Veetil, M. K.; Keller, T. M. Polymers made from polyhedral oligomeric silsesquioxanes and diacetylene-containing compounds, acetylene compounds and crosslinked product. 2009-427084 2010267913, 20090421., 2010.
20. Choi, J.; Kim, S. G.; Laine, R. M., Organic/Inorganic Hybrid Epoxy Nanocomposites from Aminophenylsilsesquioxanes. *Macromolecules* **2004,** *37* (1), 99-109.
21. (a) Choi, J.; Tamaki, R.; Kim, S. G.; Laine, R. M., Organic/Inorganic Imide Nanocomposites from Aminophenylsilsesquioxanes. *Chem. Mater.* **2003,** *15* (17), 3365-3375; (b) Tamaki, R.; Choi, J.; Laine, R. M., A Polyimide Nanocomposite from Octa(aminophenyl)silsesquioxane. *Chem. Mater.* **2003,** *15* (3), 793-797.
22. (a) Kim, K.-M.; Chujo, Y., Synthesis and characterization of liquid-crystalline silsesquioxanes. *Polym. Bull. (Berlin, Ger.)* **2001,** *46* (1), 15-21; (b) Unno, M.; Suto, A.; Takada, K.; Matsumoto, H., Synthesis of ladder and cage silsesquioxanes from 1,2,3,4-tetrahydroxycyclotetrasiloxane. *Bull. Chem. Soc. Jpn.* **2000,** *73* (1), 215-220; (c) Cordes, D. B.; Lickiss, P. D.; Rataboul, F., Recent Developments in the Chemistry of Cubic Polyhedral Oligosilsesquioxanes. *Chemical Reviews (Washington, DC, United States)* **2010,** *110* (4), 2081-2173; (d) Lickiss, P. D.; Rataboul, F., Fully condensed polyhedral oligosilsesquioxanes (POSS): from synthesis to application. *Advances in Organometallic Chemistry* **2008,** *57*, 1-116.
23. Shawn, P. H., Hybrid POSS-polymer technology for rocket & space application. *AFRL/PRSM - polymer working group propulsion sciences division* **1999**.
24. (a) Feher, F. J.; Phillips, S. H.; Ziller, J. W., Synthesis and structural characterization of a remarkably stable, anionic, incompletely condensed silsesquioxane framework. *Chem. Commun. (Cambridge)* **1997,** (9), 829-830; (b) Feher, F. J.; Budzichowski, T. A.; Rahimian, K.; Ziller, J. W., Reactions of incompletely-condensed silsesquioxanes with pentamethylantimony: a new synthesis of metallasilsesquioxanes with important implications for the chemistry of silica surfaces. *J. Am. Chem. Soc.* **1992,** *114* (10), 3859-3866; (c) Feher, F. J.; Newman, D. A.; Walzer, J. F., Silsesquioxanes as models for silica surfaces. *J. Am. Chem. Soc.* **1989,** *111* (5), 1741-1748.
25. Abbenhuis, H. C. L.; Krijnen, S.; van Santen, R. A., Modeling the active sites of heterogeneous titanium epoxidation catalysts using titanium silasesquioxanes: insight into specific factors that determine leaching in liquid-phase processes. *Chem. Commun. (Cambridge)* **1997,** (3), 331-332.
26. Murugavel, R.; Chandrasekhar, V.; Roesky, H. W., Discrete Silanetriols: Building Blocks for Three-Dimensional Metallasiloxanes. *Acc. Chem. Res.* **1996,** *29* (4), 183-189.
27. Haddad, T. S.; Mather, P. T.; Jeon, H. G.; Chun, S. B.; Phillips, S. H., Hybrid inorganic/organic diblock copolymers - Nanostructure in polyhedral oligomeric silsesquioxane polynorbornenes. *Mater. Res. Soc. Symp. Proc.* **2001,** *628* (Organic/Inorganic Hybrid Materials), CC2 6 1-CC2 6 7.

28. Knight, P. T.; Lee, K. M.; Chung, T.; Mather, P. T., PLGA-POSS End-Linked Networks with Tailored Degradation and Shape Memory Behavior. *Macromolecules (Washington, DC, U. S.)* **2009,** *42* (17), 6596-6605.
29. Lichtenhan, J. D.; Otonari, Y. A.; Carr, M. J., Linear Hybrid Polymer Building Blocks: Methacrylate-Functionalized Polyhedral Oligomeric Silsesquioxane Monomers and Polymers. *Macromolecules* **1995,** *28* (24), 8435-7.
30. Tant, M. R.; Wilkes, G. L., Physical aging studies of styrene-butadiene and carbonate-siloxane block copolymers. *Polym. Eng. Sci.* **1981,** *21* (6), 325-330.
31. Pyun, J.; Matyjaszewski, K.; Wu, J.; Kim, G.-M.; Chun, S. B.; Mather, P. T., ABA triblock copolymers containing polyhedral oligomeric silsesquioxane pendant groups: synthesis and unique properties. *Polymer* **2003,** *44* (9), 2739-2750.
32. Fu, B. X.; Hsiao, B. S.; Pagola, S.; Stephens, P.; White, H.; Rafailovich, M.; Sokolov, J.; Mather, P. T.; Jeon, H. G.; Phillips, S.; Lichtenhan, J.; Schwab, J., Structural development during deformation of polyurethane containing polyhedral oligomeric silsesquioxanes (POSS) molecules. *Polymer* **2000,** *42* (2), 599-611.
33. Karabiyik, U.; Paul, R.; Swift, M. C.; Esker, A. R., Nanofiller effects on glass transition temperatures of ultrathin polymer films and bulk blends. *PMSE Prepr.* **2008,** *98*, 863-864.
34. Yin, W.; Huffer, S. M.; Deng, J.; Hottle, J. R.; Kim, H.-J.; Esker, A. R., Dilational viscoelastic behavior in two-dimensional polymer systems with nanofillers. *Polym. Prepr. (Am. Chem. Soc., Div. Polym. Chem.)* **2007,** *48* (1), 674-675.
35. (a) Paul, R.; Karabiyik, U.; Swift, M. C.; Esker, A. R., Phase Separation in Poly(tert-butyl acrylate)/Polyhedral Oligomeric Silsesquioxane (POSS) Thin Film Blends. *Langmuir* **2008,** *24* (9), 5079-5090; (b) Paul, R.; Karabiyik, U.; Swift, M. C.; Hottle, J. R.; Esker, A. R., Morphological Evolution in Dewetting Polystyrene/Polyhedral Oligomeric Silsesquioxane Thin Film Bilayers. *Langmuir* **2008,** *24* (9), 4676-4684; (c) Hosaka, N.; Otsuka, H.; Hino, M.; Takahara, A., Control of Dispersion State of Silsesquioxane Nanofillers for Stabilization of Polystyrene Thin Films. *Langmuir* **2008,** *24* (11), 5766-5772; (d) Mitsuishi, M.; Zhao, F.; Kim, Y.; Watanabe, A.; Miyashita, T., Preparation of Ultrathin Silsesquioxane Nanofilms via Polymer Langmuir-Blodgett Films. *Chem. Mater.* **2008,** *20* (13), 4310-4316.
36. (a) Lorenz-Haas, C.; Muller-Buschbaum, P.; Kraus, J.; Bucknall, D. G.; Stamm, M., Nucleated dewetting of thin polymer films. *Appl. Phys. A: Mater. Sci. Process.* **2002,** *74* (Suppl., Pt. 1), S383-S385; (b) Xie, R.; Karim, A.; Douglas, J. F.; Han, C. C.; Weiss, R. A., Spinodal Dewetting of Thin Polymer Films. *Physical Review Letters* **1998,** *81* (6), 1251-1254; (c) Kumar, S.; Matar, O. K., Dewetting of thin liquid films near soft elastomeric layers. *J. Colloid Interface Sci.* **2004,** *273* (2), 581-588.
37. Lee, A.; Lichtenhan, J. D., Viscoelastic Responses of Polyhedral Oligosilsesquioxane Reinforced Epoxy Systems. *Macromolecules* **1998,** *31* (15), 4970-4974.
38. Fu, B. X.; Namani, M.; Lee, A., Influence of phenyltrisilanol polyhedral silsesquioxane on properties of epoxy network glasses. *Polymer* **2003,** *44* (25), 7739-7747.
39. www.chem1.com/acad/webtext/states/liquids.html.
40. Gaines, G. L., Jr., *Insoluble Monolayers at Liquid-Gas Interfaces*. 1966; p 386 pp.
41. Petty, M. C., *Langmuir-Blodgett Films; Cambridge University Press* **1996**.
42. Peterson, I. R., Langmuir-Blodgett films. *J. Phys. D: Appl. Phys.* **1990,** *23* (4), 379-395.
43. (a) Galletti, G. S.; Guiseppi-Elie, A., Vinyl stearate monolayers for Langmuir-Blodgett film applications. *Thin Solid Films* **1985,** *132*, 163-172; (b) Lloyd, J. P.; Petty, M. C.; Roberts, G. G.; Lecomber, P. G.; Spear, W. E., Amorphous silicon/Langmuir-Blodgett film field effect transistor. *Thin Solid Films* **1983,** *99* (1-3), 297-304.
44. Dynarowicz-Latka, P.; Dhanabalan, A.; Oliveira, O. N., Modern physicochemical research on Langmuir monolayers. *Adv. Colloid Interface Sci.* **2001,** *91* (2), 221-293.

45. (a) Young, T., *Phil. Trans. Roy. Soc. London* **1805,** *95*, 65; (b) de Laplace, P. S., *Mecanique Celeste, suppl. au X. Livre, Crouier, Paris* **1805**.
46. www.people.eku.edu/ritchisong/554notes1.html.
47. (a) Knobler, C. M., Seeing phenomena in flatland: studies of monolayers by fluorescence microscopy. *Science (Washington, D. C., 1883-)* **1990,** *249* (4971), 870-874; (b) Kaganer, V. M.; Mohwald, H.; Dutta, P., Structure and phase transitions in Langmuir monolayers. *Rev. Mod. Phys.* **1999,** *71* (3), 779-819; (c) Kaganer, V. M.; Peterson, I. R.; Kenn, R. M.; Shih, M. C.; Durbin, M.; Dutta, P., Tilted phases of fatty acid monolayers. *J. Chem. Phys.* **1995,** *102* (23), 9412-9422.
48. Pallas, N. R.; Pethica, B. A., Liquid-expanded to liquid-condensed transition in lipid monolayers at the air/water interface. *Langmuir* **1985,** *1* (4), 509-513.
49. Stine, K. J.; Stratmann, D. T., Fluorescence microscopy study of Langmuir monolayers of stearylamine. *Langmuir* **1992,** *8* (10), 2509-14.
50. Werkman, P. J.; Wilms, H.; Wieringa, R. H.; Schouten, A. J., Formation of mono- and multilayers of metal complexes of 4-(((10,12-pentacosadiynoyl)oxy)methyl)pyridine. *Thin Solid Films* **1998,** *325* (1,2), 238-245.
51. Fu, J. A.; Cheng, Q.; Stevens, R., Epi-fluorescence microscopic and monolayer studies of four amino acid functionalized diacetylene lipids. *Berkeley Scientific* **1998,** *2* (2), 99-103.
52. Wang, R.; Parikh, A. N.; Beers, J. D.; Shreve, A. P.; Swanson, B., Nonequilibrium Pattern Formation in Langmuir-Phase Assisted Assembly of Alkylsiloxane Monolayers. *J. Phys. Chem. B* **1999,** *103* (46), 10149-10157.
53. Zhai, X.; Brezesinski, G.; Moehwald, H.; Li, J., Thermodynamics and Structures of Amide Phospholipid Monolayers. *J. Phys. Chem. B* **2004,** *108* (35), 13475-13480.
54. (a) Ni, S.; Lee, W.; Li, B.; Esker, A. R., Thermodynamics of the Liquid Expanded to Condensed Phase Transition of Poly(L-lactic acid) in Langmuir Monolayers. *Langmuir* **2006,** *22* (8), 3672-3677; (b) Ni, S.; Satija, S. K.; Esker, A. R., Surface patterns of poly(L-lactic acid) 103 helices at the air/water interface and on solid substrates. *PMSE Prepr.* **2005,** *93*, 436-437.
55. Yue, X.; Dobner, B.; Iimura, K.; Kato, T.; Moehwald, H.; Brezesinski, G., Weak First-Order Tilting Transition in Monolayers of Mono- and Bipolar Docosanol Derivatives. *J. Phys. Chem. B* **2006,** *110* (44), 22237-22244.
56. Kaganer, V. M.; Loginov, E. B., Symmetry and phase transitions in Langmuir monolayers: The Landau theory. *Physical Review E: Statistical Physics, Plasmas, Fluids, and Related Interdisciplinary Topics* **1995,** *51* (3-A), 2237-49.
57. Overbeck, G. A.; Hoenig, D.; Moebius, D., Visualization of first- and second-order phase transitions in eicosanol monolayers using Brewster angle microscopy. *Langmuir* **1993,** *9* (2), 555-560.
58. (a) Miller, A.; Moehwald, H., Diffusion limited growth of crystalline domains in phospholipid monolayers. *J. Chem. Phys.* **1987,** *86* (7), 4258-65; (b) Suresh, K. A.; Nittmann, J.; Rondelez, F., Pattern formation during phase transition in Langmuir monolayers near critical temperature. *Europhysics Letters* **1988,** *6* (5), 437-43; (c) Hossain, M. M.; Kato, T., Line tension induced instability of condensed domains formed in adsorbed monolayers at the air-water interface. *Langmuir* **2000,** *16* (26), 10175-10183.
59. Mann, E. K.; Langevin, D., Poly(dimethylsiloxane) molecular layers at the surface of water and of aqueous surfactant solutions. *Langmuir* **1991,** *7* (6), 1112-1117.
60. Honig, E. P., Molecular constitution of X- and Y-type Langmuir-Blodgett films. *J. Colloid Interface Sci.* **1973,** *43* (1), 66-72.
61. Holley, C.; Bernstein, S., Grating space of barium copper stearate films. *Phys. Rev.* **1937,** *52*, 525-530.
62. Fox, H. W.; Zisman, W. A., Some advances in techniques for the study of adsorbed monolayers at the liquid-air interface. *Rev. Sci. Instrum.* **1948,** *19*, 274-283.

63. (a) Hoenig, D.; Moebius, D., Direct visualization of monolayers at the air-water interface by Brewster angle microscopy. *J. Phys. Chem.* **1991,** *95* (12), 4590-4592; (b) Henon, S.; Meunier, J., Microscope at the Brewster angle: direct observation of first-order phase transitions in monolayers. *Rev. Sci. Instrum.* **1991,** *62* (4), 936-939; (c) Siegel, S.; Hoenig, D.; Vollhardt, D.; Moebius, D., Direct observation of three-dimensional transformation of insoluble monolayers. *J. Phys. Chem.* **1992,** *96* (20), 8157-8160.
64. Derude, *Annu. Rev. Phys. Chem.* **1891,** *43*, 126.
65. (a) Deng, J.; Viers, B. D.; Esker, A. R.; Anseth, J. W.; Fuller, G. G., Phase Behavior and Viscoelastic Properties of Trisilanolcyclohexyl-POSS at the Air/Water Interface. *Langmuir* **2005,** *21* (6), 2375-2385; (b) Li, B.; Esker, A. R., Blends of Poly(e-caprolactone) and Intermediate Molar Mass Polystyrene as Langmuir Films at the Air/Water Interface. *Langmuir* **2007,** *23* (2), 574-581; (c) Li, B.; Wu, Y.; Liu, M.; Esker Alan, R., Brewster angle microscopy study of poly(epsilon-caprolactone) crystal growth in Langmuir films at the air/water interface. *Langmuir : the ACS journal of surfaces and colloids* **2006,** *22* (11), 4902-4905; (d) Li, B.; Marand, H.; Esker, A. R., Dendritic growth of poly(e-caprolactone) crystals from compatible blends with poly(t-butyl acrylate) at the air/water interface. *J. Polym. Sci., Part B: Polym. Phys.* **2007,** *45* (24), 3300-3318; (e) Deng, J.; Hottle, J. R.; Polidan, J. T.; Kim, H.-J.; Farmer-Creely, C. E.; Viers, B. D.; Esker, A. R., Polyhedral Oligomeric Silsesquioxane Amphiphiles: Isotherm and Brewster Angle Microscopy Studies of Trisilanolisobutyl-POSS at the Air/Water Interface. *Langmuir* **2004,** *20* (1), 109-115; (f) Deng, J.; Polidan, J. T.; Hottle, J. R.; Farmer-Creely, C. E.; Viers, B. D.; Esker, A. R., Polyhedral Oligomeric Silsesquioxanes: A New Class of Amphiphiles at the Air/Water Interface. *J. Am. Chem. Soc.* **2002,** *124* (51), 15194-15195; (g) Deng, J.; Farmer-Creely Catherine, E.; Viers Brent, D.; Esker Alan, R., Unique rodlike surface morphologies in trisilanolcyclohexyl polyhedral oligomeric silsesquioxane films. *Langmuir* **2004,** *20* (7), 2527-2530.
66. Ni, S., POLY(L-LACTIC ACID) LANGMUIR MONOLAYERS AT THE AIR/WATER INTERFACE AND LANGMUIR-BLODGETT FILMS ON SOLID SUBSTRATES: PHASE BEHAVIOR, SURFACE MORPHOLOGY, AND CRYSTALLINITY. *Ph. D. thesis at Virginia Tech* **2006**.
67. (a) Hottle, J. R.; Deng, J.; Kim, H.-J.; Farmer-Creely, C. E.; Viers, B. D.; Esker, A. R., Blends of Amphiphilic Poly(dimethylsiloxane) and Nonamphiphilic Octaisobutyl-POSS at the Air/Water Interface. *Langmuir* **2005,** *21* (6), 2250-2259; (b) Yin, W.; Deng, J.; Esker, A. R., Surface Rheology of Trisilanolisobutyl-POSS at the Air/Water Interface. *Langmuir* **2009,** *25* (13), 7181-7184.
68. Williams, A. A.; Sugandhi, E. W.; Macri, R. V.; Falkinham, J. O., III; Gandour, R. D., Antimicrobial activity of long-chain, water-soluble, dendritic tricarboxylato amphiphiles. *Journal of Antimicrobial Chemotherapy* **2007,** *59* (3), 451-458.
69. Deng, J., Interfacial characterization of polyhedral oligomeric silsesquioxane (POSS) amphiphiles and polymer blends: thermodynamics, morphology, and rheology, Ph. D. thesis, Virginia Polytechnic Institute and State Univeristy, Blacksburg, VA. **2005**.
70. (a) Wang, Y.; Cardona, C. M.; Kaifer, A. E., Molecular Orientation Effects on the Rates of Heterogeneous Electron Transfer of Unsymmetric Dendrimers. *J. Am. Chem. Soc.* **1999,** *121* (41), 9756-9757; (b) Zhang, H.; Dubin, P. L.; Kaplan, J.; Moorefield, C. N.; Newkome, G. R., Dissociation of Carboxyl-Terminated Cascade Polymers: Comparison with Theory. *J. Phys. Chem. B* **1997,** *101* (18), 3494-3497.
71. Macri, R. V.; Karlovska, J.; Doncel, G. F.; Du, X.; Maisuria, B. B.; Williams, A. A.; Sugandhi, E. W.; Falkinham, J. O., III; Esker, A. R.; Gandour, R. D., Comparing anti-HIV, antibacterial, antifungal, micellar, and cytotoxic properties of tricarboxylato dendritic amphiphiles. *Bioorganic & Medicinal Chemistry* **2009,** *17* (8), 3162-3168.
72. (a) Kim, H.-J.; Deng, J.; Lalli, J. H.; Riffle, J. S.; Viers, B. D.; Esker, A. R., Blends of Amphiphilic Trisilanolisobutyl-POSS and Phosphine Oxide Substituted Poly(dimethylsiloxane) at the Air/Water Interface. *Langmuir* **2005,** *21* (5), 1908-1916; (b) Ferguson-McPherson, M. K.; Low, E. R.; Esker, A. R.; Morris, J. R., Sorption of Dimethyl Methylphosphonate within Langmuir-Blodgett Films of

Trisilanolphenyl Polyhedral Oligomeric Silsesquioxane. *J. Phys. Chem. B* **2005,** *109* (40), 18914-18920; (c) Paul, R.; Swift, M. C.; Hottle, J. R.; Esker, A. R., Instability and dewetting of polystyrene/polyhedral oligomeric silsesquioxane (POSS) bilayer films. *PMSE Prepr.* **2006,** *94*, 778-779; (d) Paul, R.; Esker Alan, R., Pattern formation in dewetting poly(tert-butyl acrylate)/polyhedral oligomeric silsesquioxane (POSS) bilayer films. *Langmuir : the ACS journal of surfaces and colloids* **2006,** *22* (16), 6734-8.

73. jmg.centerblog.net/3455607-L-Atomium-Belgique.

74. (a) Haddad, T. S.; Lichtenhan, J. D., Hybrid Organic-Inorganic Thermoplastics: Styryl-Based Polyhedral Oligomeric Silsesquioxane Polymers. *Macromolecules* **1996,** *29* (22), 7302-7304; (b) Jeon, H. G.; Mather, P. T.; Haddad, T. S., Shape memory and nanostructure in poly(norbornyl-POSS) copolymers. *Polym. Int.* **2000,** *49* (5), 453-457; (c) Lichtenhan, J. D.; Otonari, Y. A.; Carr, M. J., Linear Hybrid Polymer Building Blocks: Methacrylate-Functionalized Polyhedral Oligomeric Silsesquioxane Monomers and Polymers. *Macromolecules* **1995,** *28* (24), 8435-8437; (d) Pescarmona, P. P.; Masters, A. F.; van der Waal, J. C.; Maschmeyer, T., Osmium silsesquioxane as model compound and homogeneous catalyst for the dihydroxylation of alkenes. *Journal of Molecular Catalysis A: Chemical* **2004,** *220* (1), 37-42.

75. Wheeler, P. A.; Fu, B. X.; Lichtenhan, J. D.; Weitao, J.; Mathias, L. J., Incorporation of metallic POSS, POSS copolymers, and new functionalized POSS compounds into commercial dental resins. *J. Appl. Polym. Sci.* **2006,** *102* (3), 2856-2862.

76. (a) Mark, J. E., Hybrid organic-inorganic composites containing mixed-oxide ceramics and high-temperature polymers. *J. Macromol. Sci., Pure Appl. Chem.* **1996,** *A33* (12, First International Polymer Symposium on Polymers from Natural Sources, 1995), 2005-2012; (b) LeBaron, P. C.; Wang, Z.; Pinnavaia, T. J., Polymer-layered silicate nanocomposites: an overview. *Appl. Clay Sci.* **1999,** *15* (1-2), 11-29; (c) Kickelbick, G.; Bauer, J.; Huesing, N., Structurally well-defined amphiphilic polysiloxane copolymers. *Silicon Chem.* **2003**, 439-450.

77. Kim, H.-J.; Lalli, J. H.; Riffle, J. S.; Viers, B. D.; Esker, A. R., Brewster angle microscopy studies of aggregate formation in blends of amphiphilic trisilanolisobutyl-POSS and nitrile substituted poly(dimethylsiloxane) at the air-water interface. *ACS Symp. Ser.* **2007,** *964* (Science and Technology of Silicones and Silicone-Modified Materials), 268-289.

78. Huffer, S. M.; Yin, W.; Esker, A. R., Limiting rheological properties of octaisobutyl-POSS and poly(dimethylsiloxane) blends. *Polym. Prepr. (Am. Chem. Soc., Div. Polym. Chem.)* **2007,** *48* (1), 717-718.